Department of Electronics

Improvement of osseointegration:

Guiding cells with external factors including a novel surface microstructure and recognizing bacterial infections

Emilia Kaivosoja

Aalto University

DOCTORAL DISSERTATIONS

Aalto University publication series
DOCTORAL DISSERTATIONS 34/2013

Improvement of osseointegration:

Guiding cells with external factors including a novel surface microstructure and recognizing bacterial infections

Emilia Kaivosoja

A doctoral dissertation completed for the degree of Doctor of Science (Technology) to be defended, with the permission of the Aalto University School of Electrical Engineering, at a public examination held at the Auditorium TU1 of the school on 15th of March 2013 at 12 noon.

Aalto University
School of Electrical Engineering
Department of Electronics

Supervising professor
Prof. Mervi Paulasto-Kröckel

Thesis advisor
Prof. Yrjö T. Konttinen, University of Helsinki

Preliminary examiners
Prof. Roel Kuijer, University of Groningen, the Netherlands
Prof. Markus Linder, Aalto University, Finland

Opponents
Prof. Roel Kuijer, University of Groningen, the Netherlands
Prof. Pekka Vallittu, University of Turku, Finland

Aalto University publication series
DOCTORAL DISSERTATIONS 34/2013

ISBN 978-952-60-5038-6 (printed)
ISBN 978-952-60-5037-9 (pdf)
ISSN-L 1799-4934
ISSN 1799-4934 (printed)
ISSN 1799-4942 (pdf)
http://urn.fi/URN:ISBN:978-952-60-5037-9

Unigrafia Oy
Helsinki 2013

Finland

441 697
Printed matter

Aalto University

Abstract

Aalto University, P.O. Box 11000, FI-00076 Aalto www.aalto.fi

Author
Emilia Kaivosoja

Name of the doctoral dissertation
Improvement of osseointegration

Publisher School of Electrical Engineering

Unit Department of Electronics

Series Aalto University publication series DOCTORAL DISSERTATIONS 34/2013

Field of research Electronics Production Technology

Manuscript submitted 9 November 2012 **Date of the defence** 15 March 2013

Permission to publish granted (date) 24 January 2013 **Language** English

☐ **Monograph** ☒ **Article dissertation (summary + original articles)**

Abstract

The aim of this study was to find methods that could potentially improve the osseointegration of an implant. The prerequisites for implant integration into bone are the adhesion of the osteoblastic cells and the ability of the progenitor cells (stem cells) to differentiate into bone cells on the surface of the implant. It was found that patterning with diamond-like carbon, Cr, Ta or Ti improved the cytocompatibility of Si substrates with osteoblastic cells and mesenchymal stem cells (MSC). The patterns affected the density of the cells, causing local cellular spots on the patterns initiating the clustering of the cells and the cell–cell contacts, which are considered necessary for osteogenesis. Indeed, patterning improved the osteogenic differentiation of MSCs compared to planar non-patterned surfaces.

With three-dimensional surfaces, the aim was to promote tissue-like growth and activation of the cytoskeleton; many previous studies have shown that this improves osteogenesis. However, this work showed that activation of the cytoskeleton alone is not osteoinductive. The osteoblastic differentiation of MSCs on 20 μm high pillars was studied, and it was found that the cytoskeleton of the cells was highly activated, but that osteogenesis was not stimulated; in fact, it was suppressed. The likely reason for this behaviour was the failure of adequate osteoinductive cell–cell contacts.

In addition to growth substrate variables, the fate of the stem cells is regulated by physical forces and soluble factors. It was found that pulsed electromagnetic fields improved the viability of the MSCs, but that they had no significant effect on their osteogenic differentiation at the relatively low seeding density used here. In contrast, a prohormone (dehydroepiandrosterone, DHEA) improved osteogenesis at least in part due to an intracrine conversion of DHEA into a sex steroid (dihydrotestosterone), but also via some other as yet undefined mechanisms.

In addition to the integration of implants with tissues via contact with other cells and extracellular matrix, another important factor regulating implant integration and the lifetime of the implant is the amount of contact it has with commensials and pathogenic microbes, in particular bacteria. Diagnostics of peri-implant infections is usually based on the bacterial culture, neutrophil infiltrates and other methods. Nonetheless, the current methods are not reliable enough. In the final part of this thesis, two methods that could potentially be utilised to diagnose implant infections were evaluated. It was found that time-of-flight secondary ion mass spectrometry is a potential tool for differentiating of acellular bacterial from eukaryotic footprints (*i.e.* extracellular polymeric substance and extracellular matrix produced by the respective cells) and may have potential for the *post-hoc* diagnosis of colonisation, biofilm formation and implant-related infections even in culture negative cases.

Keywords Osseointegration, microfabrication, pulsed electromagnetic fields, dehydroepiandrosterone, ToF-SIMS

ISBN (printed) 978-952-60-5038-6 **ISBN (pdf)** 978-952-60-5037-9

ISSN-L 1799-4934 **ISSN (printed)** 1799-4934 **ISSN (pdf)** 1799-4942

Location of publisher Espoo **Location of printing** Helsinki **Year** 2013

Pages 180 **urn** http://urn.fi/URN:ISBN:978-952-60-5037-9

Aalto-yliopisto

Tiivistelmä

Aalto-yliopisto, PL 11000, 00076 Aalto www.aalto.fi

Tekijä
Emilia Kaivosoja

Väitöskirjan nimi
Osseointegraation edistäminen

Julkaisija Sähkötekniikan korkeakoulu

Yksikkö Elektroniikan laitos

Sarja Aalto University publication series DOCTORAL DISSERTATIONS 34/2013

Tutkimusala Elektroniikan tuotantotekniikka

Käsikirjoituksen pvm 09.11.2012 **Väitöspäivä** 15.03.2013

Julkaisuluvan myöntämispäivä 24.01.2013 **Kieli** Englanti

☐ **Monografia** ☒ **Yhdistelmäväitöskirja (yhteenveto-osa + erillisartikkelit)**

Tiivistelmä

Tämän väitöskirjan tavoitteena oli kehittää menetelmiä, joilla implantin kiinnittymistä luuhun voidaan edistää. Implantin kudosintegraation kannalta on tärkeää, että solut kiinnittyvät implantin pintaan ja että kantasolut kykenevät erilaistumaan luusoluiksi implantin pinnalla. Tutkimuksessa havaittiin, että kun piin pinta kuvioitiin eri materiaaleilla (timantinkaltainen hiili, Cr, Ta tai Ti), bioyhteensopivuus luusolujen ja kantasolujen kanssa parani. Kuviot edesauttoivat solujen paikallista konsentroitumista, mikä voi aiheuttaa soluryppäiden syntymisen ja edesauttaa solujen välisiä kontakteja, jotka ovat edellytyksenä osteogeneesille. Kuvioidun pinnan havaittiinkin edistävän luunmuodostusta verrattuna sileään pintaan.

Kolmiulotteisten pintojen avulla tavoitteena oli tukea solujen kolmiulotteista kasvua ja solutukirangan aktivoitumista, jonka on todettu edistävän luunmuodostusta lukuisissa aikaisemmissa tutkimuksissa. Tässä tutkimuksessa kuitenkin havaittiin, että pelkkä tukirangan aktivoituminen ei riitä aiheuttamaan luunmuodostusta. Kantasolujen erilaistumista tutkittiin pilaripinnoilla, joilla 20 μm pilareihin kiinnittyneiden solujen tukiranka aktivoitui voimakkaasti, mutta luunmuodostus oli kontrolleihin verrattuna vähäistä. Tähän todennäköisenä syynä oli kiinnittymiskohtiensa välillä venyvien yksinäisten solujen välisten kontaktien vähäisyys, mitkä myös ovat välttämättömiä luunmuodostukselle.

Materiaalin lisäksi kantasolujen erilaistumiseen voidaan vaikuttaa fysikaalisilla voimilla ja liukoisilla tekijöillä. Tutkimus osoitti pulssitettujen sähkömagneettisten kenttien edistävän solujen eloonjäämistä ja jakautumista, mutta luun muodostuksessa kentillä ei ollut vaikutusta kokeissa käytetyillä alhaisilla solutiheyksillä. Sukupuolihormonien esiasteen, dehydroepiandrosteroinin, havaittiin muokkautuvan soluissa aktiiviseksi sukupuolihormoniksi (dihydrotestosteroniksi) ja edistävän luunmuodostusta, mutta tukevan luunmuodostusta jossain määrin myös joidenkin muiden mekanismien kautta.

Kudoskontaktin lisäksi toinen merkittävä seikka, joka vaikuttaa implantin integroitumiseen ja elinikään, on kontakti normaalin mikrobiflooran ja patogeenien kanssa. Bakteeri-infektioiden diagnosoiminen nykyisillä bakteeriviljelyihin, neutrofiilikertymiin ja muihin seikkoihin perustuvilla menetelmillä ei ole kyllin luotettavaa. Väitöskirjan viimeisessä osiossa tutkittiin kahta potentiaalista uutta menetelmää bakteeri-infektioiden tunnistamiseen. Lentoaikaerotteisella sekundaari-ioni massaspektrometrilla (ToF-SIMS) oli mahdollista erottaa bakteerien tuottamat jalanjäljet (solunulkoinen polymeerinen aines) eukaryoottisolujen tuottamista jalanjäljistä (soluväliaine). Väärien negatiivisten bakteeriviljelyiden osalta ToF-SIMS menetelmällä on potentiaalia implantin pinnalla esiintyneiden bakteeri-infektioiden osoittamiseen.

Avainsanat Osseointegraatio, mikrovalmistus, pulssitetut magneettikentät, dehydroepiandrosteroni, ToF-SIMS

ISBN (painettu) 978-952-60-5038-6 **ISBN (pdf)** 978-952-60-5037-9

ISSN-L 1799-4934 **ISSN (painettu)** 1799-4934 **ISSN (pdf)** 1799-4942

Julkaisupaikka Espoo **Painopaikka** Helsinki **Vuosi** 2013

Sivumäärä 180 **urn** http://urn.fi/URN:ISBN:978-952-60-5037-9

Preface

The studies described in this thesis were carried out at the Department of Clinical Medicine, Helsinki University Central Hospital. This study was supported by Finska Läkaresällskapet, Aalto University, the National Doctoral Programme of Musculoskeletal Diseases and Biomaterials, the Finnish Cultural Foundation, the Orion-Farmos Research Foundation, the Biomedicum Helsinki Foundation, Biocentrum Helsinki, the Otto A. Malm Foundation and the Orton Research Institute.

There are many people to thank, and I hereby wish to sincerely acknowledge everybody who has contributed to this work in one way or another. Especially, I would like to thank Prof. Yrjö Konttinen for taking me under his wing and nourishing me with science, for inspiring and challenging me and for having a great deal of confidence in me. Yrjö had an endless number of ideas and a clever explanation for whatever result we got, but he also has a big heart. I owe sincere and heartfelt thanks to my supervisor, Prof. Mervi Paulasto, for her valuable comments and words of encouragement. Her insightful suggestions and constructive comments have greatly improved this summary.

Prof. Roel Kuijer is warmly thanked for reviewing this thesis and for kindly agreeing to be my opponent. Prof. Pekka Vallittu is also deeply thanked for kindly agreeing to be my opponent. Prof. Markus Liner receives my grateful acknowledgements for reviewing this thesis.

Prof. Sannakaisa Virtanen gave me an opportunity to visit the Department of Materials Science and Engineering (WW-4, LKO), at the University of Erlangen-Nuremberg in Germany, for which I am extremely grateful. I would like to thank Helga Hildebrand and Anja Friedrich for doing the ToF-SIMS, XPS and SEM measurements with me.

I wish to thank Dr. Riina Richardson for introducing me to bacteriology and letting me use her lab. The late Prof. Ismo Virtanen is acknowledged

for his invaluable help with the cell work and antibodies. I also wish to thank Prof. Michiaki Takagi for his encouragement along the way.

I want to express my sincere thanks to the Kuopio-team, Prof. Reijo Lappalainen, Sami Myllymaa, Katja Myllymaa and Hannu Korhonen, for fabricating the micropatterned samples and to the microfabrication team, Prof. Sami Franssila, Pia Suvanto and Susanna Aura, for fabricating the 3D-samples.

I want to thank Prof. Maria-Pau Ginebra for giving me the opportunity to visit the Department of Materials Science and Metallurgy, at the Technical University of Catalonia in Barcelona, Spain and Montserrat Español Pons for helping me to do the ζ-potential measurements there and sharing some of the best parts of Barcelona with me.

This thesis would not have been possible without the expert guidance and precious help of all my colleagues who were involved in the study. Mari is always willing to help and extremely patient with everybody, and I want to thank her for the good advice she has given and for sharing a great time with me in Paris. I am thankful to Vesa-Petteri for getting me started with this project and to Jukka for teaching me about cell culture and for sharing a great time with me in Zabrze. I would like to show my gratitude to Erkki for his invaluable help with the staining and for many interesting discussions. I would like to acknowledge Jami for having a great deal of patience in helping me especially with PCR and for sharing his insights and expertise. I want to thank Pauliina, who not only gets along with everybody but also makes friends with everybody, for cheering us all up with her positive attitude. Eija kept the lab in order, for which my mere expression of thanks likewise does not suffice. I am most grateful to Veikko for his great help with the PEMF & DHEA experiments and to Gonçalo for his help with the 3D experiment and for sharing his enthusiasm of a junior researcher. Many thanks to Antti for doing some of the DLC coatings and shipping the samples. I want to thank Hanna-Mari for keeping the practical things going and for helping us all in so many ways. I would like to thank all other current and former members of the TULES group: Ahmed, Hakim, Katja, Liisa, Kalle, Vasily, Yan, Yuya, Noe, Tarvo, Nina, and everybody else. I have honestly enjoyed working with you and you have all made these years special for me.

I express my gratitude to all of the personnel of the EILB group for the warm and creative work environment and the fun times.

Huge thanks got out to all the friends that I met during the nearly nine

years spent at HUT and Aalto for all the great memories. In particular, I want to thank Päivikki for sharing all the pain and all the joy with me.

I am ever grateful to my parents for their continuous support and encouragement along the way: to Mom for pushing me forward, and to Dad for understanding everything without any words said.

Kristiina and Jere, without you I could not have completed my thesis. Seriously, Kristiina taught me to read and Jere taught me to calculate. More importantly, you have always been a role model for me and your example and advice have been incredibly important for me.

And Tomi, you make me happy every day. Pulpul.

Helsinki, February 5, 2013,

Emilia Kaivosoja

Nainen tarvitsee elämässään kahta asiaa: huumoria ja punaiset korkokengät.

-- Tohtorin tutkinto on hyväksi, muttei välttämätön.

Riikka Pulkkinen, Totta

Contents

List of Publications

This thesis consists of an overview and of the following publications which are referred to in the text by their Roman numerals.

I E Kaivosoja, S Myllymaa, V-P Kouri, K Myllymaa, R Lappalainen and YT Konttinen. Enhancement of silicon using micro-patterned surfaces of thin films. *Eur Cell Mater*, 19:147–157, April 2010.

II S Myllymaa, **E Kaivosoja**, K Myllymaa, H Korhonen, R Lappalainen and YT Konttinen. Adhesion, spreading and osteogenic differentiation of mesenchymal stem cells cultured on micropatterned amorphous diamond, titanium, tantalum and chromium coatings on silicon. *J Mater Sci Mater Med*, 21:329–341, August 2009.

III E Kaivosoja, S Myllymaa, Y Takakubo, H Korhonen, K Myllymaa, YT Konttinen, R Lappalainen and M Takagi. Osteogenesis of human mesenchymal stem cells on micro-patterned surfaces. Accepted for publication in *J Biomater Appl*, November 2011.

IV E Kaivosoja, P Suvanto, G Barreto, S Aura, A Soininen, S Franssila and YT Konttinen. Cell adhesion and osteogenic differentiation on three-dimensional pillar surfaces. *J Biomed Mater Res A*, 101A:842–852, July 2012.

V E Kaivosoja, V Sariola, Y Chen and YT Konttinen. The effect of pulsed electromagnetic fields and dehydroepiandrosterone on viability and osteoinduction of human mesenchymal stem cells. Accepted for publication in *J Tissue Eng Regen Med*, August 2012.

VI E Kaivosoja, S Virtanen, R Rautemaa, R Lappalainen and YT Konttinen. Spectroscopy in the analysis of bacterial and eukaryotic cell footprints on implant surfaces. *Eur Cell Mater*, 24:60–73, July 2012.

Author's Contribution

Publication I: "Enhancement of silicon using micro-patterned surfaces of thin films"

The author defined the research plan together with the co-authors. The experimental work and data analysis for the cellular studies was planned and carried out by the author, with contributions from V.-P. Kouri. The author and Professor Konttinen chiefly wrote the paper, assisted by S. Myllymaa and Professor Lappalainen.

Publication II: "Adhesion, spreading and osteogenic differentiation of mesenchymal stem cells cultured on micropatterned amorphous diamond, titanium, tantalum and chromium coatings on silicon"

The author defined the research plan together with the co-authors. The experimental work and data analysis for the cellular studies was planned and carried out by the author. The author and S. Myllymaa contributed equally to preparing the results and writing the paper, assisted by Professors Lappalainen and Konttinen.

Publication III: "Osteogenesis of human mesenchymal stem cells on micro-patterned surfaces"

The author defined the research plan together with Professor Konttinen. The experimental work and data analysis for the cellular studies and zeta potential measurements was planned and carried out by the author and she had a major role in writing the manuscript.

Publication IV: "Cell adhesion and osteogenic differentiation on three-dimensional pillar surfaces"

The author defined the research plan together with the co-authors. The experimental work (except for the material fabrication) was either carried by the author or done under her supervision. The data analysis was planned and carried out by the author and she had a major role in writing the manuscript.

Publication V: "The effect of pulsed electromagnetic fields and dehydroepiandrosterone on viability and osteoinduction of human mesenchymal stem cells"

The author defined the research plan together with Professor Konttinen. The experimental work was either planned and carried out by the author or done under her supervision. The data-analysis was carried out by the author and she had a major role in writing the manuscript.

Publication VI: "Spectroscopy in the analysis of bacterial and eukaryotic cell footprints on implant surfaces"

The author defined the research plan together with Professor Konttinen. The cell and bacterial cultures were performed by the author and she participated in the SEM, XPS and the ToF-SIMS measurements. Data analysis related to the ToF-SIMS measurement was carried out by the author and she had a major role in writing the manuscript.

Nomenclature

ALP	Alkaline phosphatase
BMP	Bone morphogenetic protein
BMPR	Bone morphogenetic protein receptor
BSA	Bovine serum albumin
BSP	Bone sialoprotein
Calmodulin	Calcium-modulated protein
COL	Collagen
DAPI	4',6-diamidino-2-phenylindole
DHEA	Dehydroepiandosterone
Dkk	Dickkopf
DLC	Diamond-like carbon
DLVO	Derjaguin & Landau and Verwey & Overbeek
ECM	Extracellular matrix
EPS	Extracellular polymeric substance
ERK	Extracellular signal-regulated kinase
FAK	Focal adhesion kinase
FBS	Foetal bovine serum
FGF	Fibroblast growth factor
FPAD	Filtered pulsed arc discharge
HA	Hydroxyapatite
IGF	Insulin-like growth factor
IHC	Immunohistochemistry
IHH	Indian hedgehog
LRP	Low-density lipoprotein receptor-related protein
MAP2K	Mitogen-activated protein kinase kinase
MAP3K	Mitogen-activated protein kinase kinase kinase
MAPK	Mitogen-activated protein kinase

MEK	Mitogen-activated protein or extracellular signal-regulated kinase kinase
MSC	Mesenchymal stem cell
MSCGM	Mesenchymal stem cell growth media
MTT	3-(4,5-Dimethylthiazol-2-yl)-2,5-diphenyltetrazolium bromide
OC	Osteocalcin
OP	Osteopontin
OPG	Osteoprotegerin
OSX	Osterix
PBS	Phosphate buffered saline
PCA	Principal component analysis
PEMF	Pulsed electromagnetic field
PFA	Paraformaldehyde
PI3K	Phosphoinositide 3-kinase
PKC	Protein kinase C
qRT-PCR	Quantitative real-time polymerase chain reaction
Raf	Rapidly accelerated fibrosarcoma
Ras	Rat sarcoma
RhoA	Ras homolog gene family, member A
ROCK	Rho-assosiated protein kinase
RPLP0	Ribosomal protein, large, P0
RUNX	Runt-related transcription factor
SaOS	Sarcoma osteogenic
SEM	Scanning electron microscopy
SMAD	Small body size and mothers against decapentaplegic-related proteins
SOX	Sry-related high motility group box
ToF-SIMS	Time-of-flight secondary ion mass spectrometry
TSB	Tryptic soy broth
XPS	X-ray photoelectron spectroscopy

List of Symbols

A	cross-section of the streaming channel
I	streaming current
L	length of the streaming channel
lr	sampling length
P	streaming pressure
V_{vdW}	electrodynamic van der Waals attraction potential
V_{tot}	net interaction potential
V_{dl}	electrostatic double-layer repulsion potential
$z(x)$	absolute profile value from a midline

ϵ	permittivity
ϵ_0	dielectric coefficient of electolyte
γ	surface tension
γ_{CS}	cell-substrate surface tension
γ_{CW}	cell-aqueous surface tension
γ_L	liquid surface tension
γ_L^D	dispersive component of the liquid surface tension
γ_L^P	polar component of the liquid surface tension
γ_S	total surface energy
γ_S^D	dispersive component of the solid surface tension
γ_S^P	polar component of the solid surface tension
γ_{SL}	solid-liquid surface tension
γ_{SW}	substrate-aqueous solution surface tension
η	electrolyte viscosity
θ	contact angle
ζ	zeta potential

1. Introduction

With an aging population and a rising trend in the number of patients in need of a joint replacement at a younger age, costly revision surgeries will become increasingly common. As an example of this trend, the total number of hip fractures almost doubled recently within just 10 years (Lönnroos *et al.*, 2006), and 14% of the hip implant operations in 2010 were revision operations (Perälä, 2011), causing an annual cost of 10 million euros in Finland. Loosening of the implant is one of the common causes of implant failure. By improving the integration of the implant to the host bone, the need for these costly revision surgeries can be reduced.

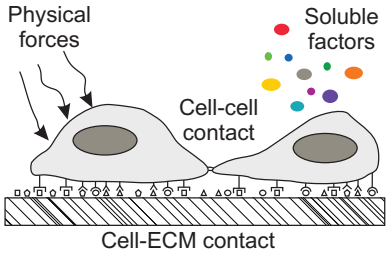

Figure 1.1. The four major factors regulating cellular behaviour, such as stem cell fate.

Improving the integration of an implant with host tissues is one of the key factors for the long-term success of implants. The prerequisites for implant integration into bone are the successful adhesion of the osteoblastic cells (osteoconduction) and the ability of the progenitor cells (stem cells) to differentiate into bone cells on the surface of the implant (osteoinduction). The stem cell fate is determined by physical forces, *e.g.* by vibration loading (Tirkkonen *et al.*, 2011), soluble factors, cell–cell contacts and cell–extracellular matrix (ECM) contact (Fig. 1.1). In addition to the regeneration of the tissue, the capacity to avoid bacterial adhesion and colonisation as well as subsequent chronic infection and inflammation, which may cause tissue necrosis, is necessary for osseointegration.

In order to regulate osseointegration, it is necessary to understand the process leading to osseointegration. Knowledge concerning the interac-

tions between cells and biomaterials is needed. In addition to cell-material interactions, the effect of a physical force (pulsed electromagnetic field, PEMF) and a soluble factor (dehydroepiandrosterone, DHEA) on bone formation are in focus. These topics are the first themes addressed in this thesis, while the last part of the literature review focuses on bacterial infections, which remain an important cause of failure for many types of implants.

The main objective of this thesis was to find methods that could potentially improve the osseointegration of an implant. This thesis examined the effect of micro-textured surfaces on osteoblastic cell adhesion, mesenchymal stem cell adhesion and osteogenic differentiation. The study was broadened to include three-dimensional surfaces, where the effect of pillars with different heights on osteoblastic cell adhesion, mesenchymal stem cell adhesion and osteogenic differentiation was studied. The study was continued by examining the effect of one physical force (PEMF) and one soluble factor (DHEA) on osteogenic differentiation. Finally, new potential methods that could be utilised in the diagnosis of implant infections were evaluated. New methods are needed because current methods are not totally reliable and because it is crucial to understand the reasons and mechanisms for implant failure in order to develop better implant materials in the future.

2. Osseointegration

The long-term clinical success of implants in contact with bone depends critically on the direct structural and functional connection between the bone and the surface of the implant. This condition is called osseointegration and it shares many prerequisites with primary fracture healing, such as precise fit, primary stability and adequate loading during the healing period. In addition, osseointegration requires a bioinert or bioactive material and surface that support and induce bone deposition.

Peri-implant tissue healing starts with an inflammatory response as the implant is inserted in the bone cavity or surface. Consequently, the released chemicals cause bone cells and progenitor cells to migrate into the site of the lesion (*i.e.* chemotaxis). Progenitor cells, *e.g.* mesenchymal stem cells (MSCs), can proliferate and differentiate into osteoblasts and begin depositing bone on the walls of the bone defect, on the fragment of the bone and on the implant surface (Schenk and Buser, 1998). This early bone response to the implant gradually develops into a so-called biological fixation of the device.

2.1 Osteogenic differentiation of mesenchymal stem cells

MSCs have been found in a variety of adult tissues, including bone marrow and fat tissue, and they have a strong proliferative potential and a capacity to form bone, cartilage, adipocytes, fibrous tissue, myoblasts, and possibly even neural tissues (Reyes and Verfaillie, 2001; Jiang *et al.*, 2002a,b, 2003). The osteogenic differentiation potential of human bone marrow MSCs may be preserved to old age (Leskelä *et al.*, 2003).

Based on bone nodule formation *in vitro*, osteogenic differentiation can be subdivided into three stages (Fig. 2.1):

1. lineage commitment and proliferation

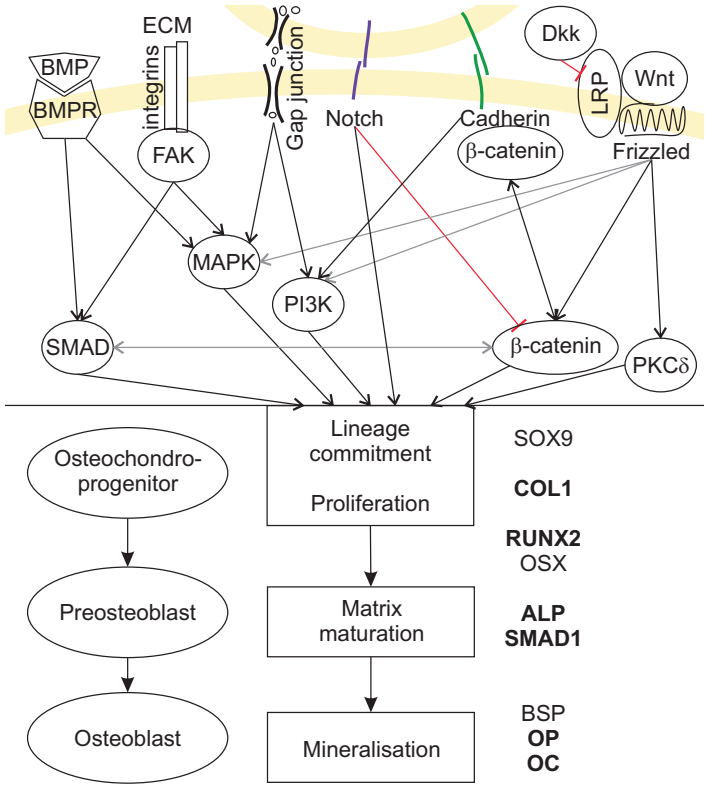

Figure 2.1. The upper half of the figure represents some of the signalling pathways involved in osteoblastogenesis. The yellow line represents the cell membrane. The lower half shows the stages of differentiation of mesenchymal stem cells as they become osteoblasts, together with some common markers of each stage (the markers that are studied in this thesis are in bold font).

2. ECM development and maturation
3. mineralisation.

This division is useful for a discussion of osteoblast biology and bone formation, but the exact characteristics of the different-stage cells are not yet well understood.

Mesenchymal progenitors that give rise to osteoblasts and chondrocytes are initially characterised by Sry-related high-motility-group box 9 (SOX9) transcription factor. During the proliferation phase, in addition to cell growth and cell cycle genes, type I collagen (COL1) genes are actively expressed. Collagen I is an important component of bone ECM; it forms connections with cell surface integrins and other ECM proteins. However, collagen I cannot be considered bone specific because it is produced by numerous non-osteoblastic cell types.

Preosteoblasts include all cells transitioning from progenitors to mature osteoblasts, and therefore, they are by definition dynamically het-

erogeneous. However, they are commonly considered to express the runt-related transcription factor 2 (RUNX2, previously known as the core binding factor alpha, Cbfa1), or at a more advanced stage of differentiation, both RUNX2 and osterix (OSX, which is also known as specificity protein 7, SP7). RUNX2 is integral to the osteoblast lineage and is indispensable for osteoblast differentiation during both intramembranous and endochondral ossification. Intramembranous ossification has to do with the direct formation of osteoblasts, while endochondral ossification involves cartilage as a precursor.

During the ECM maturation phase, both alkaline phosphatase (ALP) and osteopontin (OP) gene expressions appear. ALP may act as an early indicator of cellular activity and differentiation, but ALP is a ubiquitous cellular protein, and consequently, it cannot be considered bone specific. The molecular markers and their order of appearance during the differentiation of the mesenchymal progenitors are still being debated.

At the onset of mineralisation, some non-collagenous proteins such as OP, bone sialoprotein (BSP) and osteoprogeterin (OPG) increase. Osteoblasts are characterised by the expression of osteocalcin (OC), which is the second most abundant protein after collagen I in bone and is one of the few osteoblast-specific gene products (Ryoo *et al.*, 1997). All of these proteins facilitate the deposition of calcium and phosphate into the ECM.

2.2 Osteogenic signalling pathways

Modulating the osteogenic differentiation requires an understanding of the signalling pathways involved in the process. When beginning this research project, the signalling pathways regulating osteogenesis had not yet been well described. In fact, they were only recently reviewed by Long (2012) and Arvidson *et al.* (2011). These reviews, however, pay little or no attention to the role of cell–substrate interactions in the regulation of osteogenic differentiation. To supplement the reviews, the following description of the osteogenic signalling pathways focuses on the role of cell–substrate interactions (Fig 2.1).

With a better understanding of osteogenesis signalling, medical experts are able to regulate osteogenic differentiation more effectively using materials and other external factors. For example, should the role of the signalling pathways be completely understood, long-term experiments would no longer be needed. Instead, the outcome could be modelled, for example,

from gene expression profiles at an early stage. Moreover, if protein adsorption and cell adhesion were completely understood, the process could be modelled in its entirety.

One of the major regulators of the cell–substrate interactions in osteogenesis is mitogen-activated protein kinase (MAPK) signalling. Publication IV, however, demonstrated the activation of a MAPK pathway that was associated with delayed bone formation (described in Section 9.3.2). Therefore, it is clear that other signalling pathways are also involved in osteogenesis. The delayed osteogenesis discussed in Publication IV was linked to the material-dependent down-regulation of cell–cell interaction. Indeed, the cell–cell interactions regulate osteogenesis via cadherins, gap junctions and Notch signalling. Future studies might, for example, investigate how three-dimensional surfaces influence these signalling pathways.

Whereas hedgehog signalling, a fibroblast growth factor (FGF) and an insulin-like growth factor (IGF) signalling regulate osteogenesis, according to current knowledge these signalling pathways are not directly linked to cell–substrate interactions and are, therefore, not described here.

2.2.1 Mitogen-activated protein kinase signalling

Nearly every extracellular ligand that regulates bone biology acts, at least in part, through MAPK pathways. Each MAPK pathway contains a three-tiered kinase cascade, which is comprised of a MAP3K (MAPK kinase kinase), a MAP2K (MAPK kinase) and a MAPK (Fig. 2.2). One of the MAPK pathways is termed a MEK/ERK pathway (mitogen-activated protein or extracellular signal-regulated kinase kinase / extracellular signal-regulated kinase).

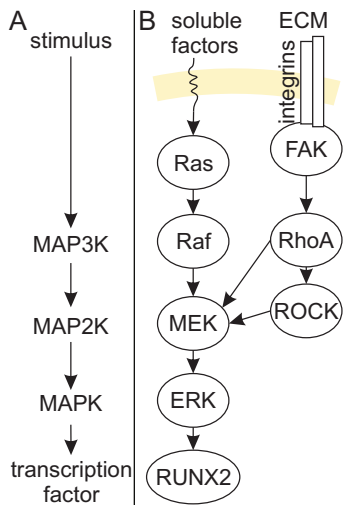

Figure 2.2. Panel A shows the general MAPK signalling, whereas panel B shows the ERK branch of the MAPK signalling and how the focal adhesion signalling is connected to the MAPK signalling. The yellow line represents a cell membrane.

At the cell-substrate contact points, specialised structures are formed and termed focal adhesions. The focal adhesion kinase (FAK) regulates

the activation of the cell cytoskeleton, including the proteins RhoA (Ras homolog gene family, member A) and ROCK (Rho-associated protein kinase). The cross-talk between the RhoA-ROCK and the MEK/ERK pathway regulates the activity of RUNX2 (Khatiwala *et al.*, 2009; Salasznyk *et al.*, 2007; Biggs *et al.*, 2009; Xiao *et al.*, 2002). This appears to be critical for MSC-mediated bone formation (Sjöström *et al.*, 2009).

2.2.2 Signalling through gap junctions

A gap junction is a specialized intercellular connection between cells. It connects the cytoplasm of two cells and allows various small molecules and ions to pass freely between the cells. Cell–cell communication through gap junctions is required for the full maturation of osteoblasts (Ferrari *et al.*, 2000; Schiller *et al.*, 2001; Li *et al.*, 1999). Second messengers, which are activated by a primary cell response to an extracellular cue, are propagated via the gap junctions. These gap junction-dependent secondary responses can activate MEK/ERK and phosphoinositide 3-kinase (PI3K) signalling (Stains and Civitelli, 2005b). The clearest demonstration of the essential role of gap junctions in bone formation has been observed in knockout mice lacking the gap junction protein connexin 43, which results in skull abnormalities, brittle, misshapen ribs and delayed mineralisation of the long bones (Lecanda *et al.*, 2000; Chung *et al.*, 2006). Gap junctional communication between osteoblasts, osteocytes and osteoclasts seems to be essential for the integrity of bone cells (Ilvesaro and Tuukkanen, 2003).

2.2.3 Notch signalling

Because the Notch receptor and its ligands are transmembrane proteins, a cell–cell interaction is required for the activation of the Notch signalling cascade. Intriguingly, the consequences of Notch activation in the cells of the osteoblast lineage are stage specific. The Notch inhibits osteoblastogenesis from early precursors by antagonising (*i.e.* counteracting) Wnt signalling (Canalis, 2008), but leads to a pathological overproduction of immature osteoblasts at a later stage (Long, 2012).

2.2.4 Cadherin-mediated cell–cell signalling

Communication between osteoblasts via N-cadherin adherent junctions is essential for endochondral bone growth. N-cadherin is important for the maintenance of the pool of bone marrow progenitor cells, and cadherin

11 is involved in osteoblast commitment and differentiation (Benedetto *et al.*, 2010). Cadherin-mediated osteoblast junction formation is linked to an activation of the PI3K signalling (Guntur *et al.*, 2012), but more importantly, cadherins regulate Wnt signalling.

2.2.5 Wnt signalling

The canonical Wnt pathway describes a series of events that ultimately results in an increase in the amount of β-catenin that reaches the nucleus. β-catenin modulates the switches between chondrogenesis and osteogenesis in the progenitor cells. The induced canonical Wnt signalling can upregulate the RUNX2 expression, which leads to osteoblast differentiation, whereas lower levels of the canonical Wnt signalling result in chondrogenesis. Intriguingly, inhibition of the canonical Wnt pathway promotes certain aspects of osteoblast development through the bone morphogenic protein (BMP)2-pathway. The Dickkoppf (Dkk) family appears to regulate this process (Fujita and Janz, 2007). Dkk1 and 2 inhibit the canonical Wnt pathway when low-density lipoprotein receptor-related protein (LRP)-Frizzled complexes are abundant (see Fig. 2.1). However, Dkk2 has a dual role and can also activate the canonical Wnt signalling at later stages of osteoblast differentiation (Olivares-Navarrete *et al.*, 2010).

Wnt signalling is partly regulated by cadherin-mediated cell–cell interaction (Stains and Civitelli, 2005a) as well as through protein kinase Cδ (PKCδ) activation (Tu *et al.*, 2007), PI3K signalling (Fukumoto *et al.*, 2001) and MAPK/ERK cascade (Yun *et al.*, 2005). Wnt signalling can also be triggered by physical forces, such as ultrasound (Olkku *et al.*, 2010).

2.2.6 Bone morphogenic protein signalling

Finally, cell–substrate interactions are linked to BMP signalling because BMP–SMAD (small body size and mothers against decapentaplegic-related protein) signalling requires FAK activity (Tamura *et al.*, 2001). BMPs play a role in osteoinductive bone formation (Waris *et al.*, 2010), and BMP2 can also be loaded into biomaterials to improve the osteoinductivity of the material (Välimäki *et al.*, 2005; Mesimäki *et al.*, 2009). Here, SMAD1 activation was demonstrated in Publications III and V. Interestingly, SMAD1/4 interacts with β-catenin, linking the BMP and Wnt pathways (Nakashima *et al.*, 2005). BMPs also stimulate osteoblast differentiation and influence how osteoblasts function via MAPK signalling.

3. The Material Properties Regulating Cellular Responses

The major material characteristics that may conceivably influence cellular responses are presented in Fig. 3.1. The properties of a material define what proteins can be adsorbed on its surface and can affect the functionality of the proteins by changing their conformation. Furthermore, cell–surface interactions regulate the formation of adhesive bonds and the subsequent activation of a specific cell programme, such as apoptosis, migration or differentiation. The cell behaviour at the interfaces is dependent upon the adsorbed molecule layers as well as the underlying substrate. Cells sense and respond to their substrate directly and can convert mechanical stimuli into chemical activity, *i.e.* mechanotransduction.

What makes biomaterial research difficult is the fact that many of the properties of a material are interconnected, and therefore, it is sometimes difficult to determine what factor plays the major role in the evoked cellular response. For example, a change in the surface chemistry or surface topography affects the surface energy. In addition, the effects of one variable can reverse the effect of another variable: for example, the fibronectin molecules adsorbed on surfaces with hydroxyl functional groups unfold and expose cell binding sites (Keselowsky *et al.*, 2003), but the morphology of the substrate can reverse this effect (Jedlicka *et al.*, 2007).

A brief summary of the effects of certain surface properties on cell adhesion, osteogenic differentiation and bone formation is presented here. Elasticity and porosity are also important regulators of stem cell fate (reviewed by Kaivosoja *et al.* (2012)), but they were not studied in the experimental settings devised for this thesis.

3.1 Surface chemistry

Surface chemistry modulates cellular responses on biomaterials primarily by regulating protein adsorption. The chemical composition of the surface

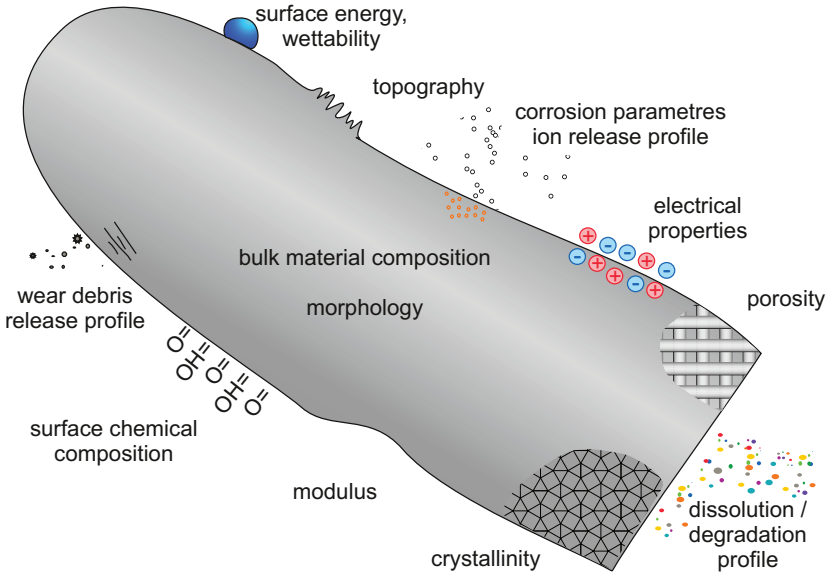

Figure 3.1. Major material characteristics that influence cellular response.

dictates the type of bonds that form between the proteins and the surface.

The differentiation of human MSCs can be directed along the desired lineages by mimicking the chemical cues present in their natural environment. The doping of hydrogels with phosphate groups that mimic mineral deposits promoted osteogenesis, whereas doping with pendant carboxyl groups that mimic the glycosaminoglycans in cartilage-enhanced chondrogenesis and doping with tert-butyl groups that resemble the lipid-rich environment in adipose tissue fostered adipogenesis (Benoit *et al.*, 2008).

A number of biomaterials possess the ability to induce bone formation, *i.e.* osteoinduction. The majority of materials described as osteoinductive contain calcium phosphate (Barradas *et al.*, 2011). Calcium phosphates are well known for their affinity for binding various proteins, including BMPs (Uludag *et al.*, 1999; Boix *et al.*, 2005) *in vivo* (Kandori *et al.*, 1997; Wallwork *et al.*, 2002). In addition, some materials that do not contain calcium phosphate, such as titanium, calcify when exposed to simulated body fluid (Fujibayashi *et al.*, 2004; Takemoto *et al.*, 2006), and therefore, they are expected to undergo a similar calcification *in vivo*.

3.2 Surface energy

The surface energy, γ, of a homogeneous substance is a measure of the energy required to form a unit area of new surface at the interface. Surface energy is dictated by the surface roughness, surface topography and

the chemical composition of the implant, and it indicates the wetting capability of the surface. For water, a relatively more wettable surface may be termed hydrophilic (high surface energy) and less wettable surfaces hydrophobic (low surface energy), respectively. A water contact angle of 65° has been determined to be the value below which surfaces are called hydrophilic and above which they are called hydrophobic (Vogler, 1998).

According to basic thermodynamic principles, a cell (C) can adhere to substrate (S) in an aqueous environment (W) if the free energy of the system decreases, *i.e.*

$$\gamma_{CS} < \gamma_{CW} + \gamma_{SW}. \tag{3.1}$$

To estimate the surface energy of materials and their components, contact angles with polar and non-polar liquids with known surface tension values are measured. However, the experimental determination of the contact angle, θ, and liquid-vapour surface tension, γ_L, of the solid-liquid-vapour system only yields a relationship between two unknown parameters, *i.e.* a solid-vapour surface tension, γ_S, and solid-liquid surface tension, γ_{SL}. According to Young's equation, the relationship is as follows:

$$\gamma_L \cos\theta = \gamma_S - \gamma_{SL}. \tag{3.2}$$

Much effort has been devoted to combining the rules so that all of the parameters can be determined. This approach has been applied successfully with some polymers and simple organic liquids. Nonetheless, the diversity of specific interactions in biological systems cannot be explained by these simplified rules. A major problem is that it is difficult to obtain accurate values for the surface free energies of cells because these surfaces possess a complex chemistry and hydration *in vivo*. This precludes doing an experimental check on any rule for combining the parameters.

Even if these parameters could be measured, the thermodynamic approach is challenging because cells are living organisms that are able to convert substances into energy, and their adhesion may be driven by energy-consuming physiological mechanisms. Moreover, the adhesion energies constitute only a small per cent of the folding energy of a molecule, such as a protein. Thus, even modest conformational changes may strongly affect molecule-to-surface interaction.

Despite the lack of a quantitative model, it is clear that surface energy regulates biological adhesion to surfaces. Generally, hydrophobic surfaces enhance the adsorption of proteins and conformational changes due to a large positive entropy change and energetically favourable bind-

ing, whereas hydrophilic surfaces decrease protein adsorption and conformational changes. Hydrophilic surfaces, on the other hand, have been shown to enhance the adhesion and spread of various cell types (Lai *et al.*, 2010; Khang *et al.*, 2008; Feng *et al.*, 2003; Sawase *et al.*, 2008). This behaviour is regulated by the adsorbed protein layer. For example, although hydrophobic surfaces adsorbed higher amounts of fibronectin than hydrophilic surfaces, the hydrophilic surfaces bound antifibronectin antibodies and supported cell adhesion more efficiently than the hydrophobic surfaces (Grinnell and Feld, 1982). Furthermore, bovine serum albumin (BSA), which inhibits cell adhesion, has been shown to adsorb more on hydrophobic surfaces (Carré and Lacarriére, 2008). In the presence of foetal bovine serum (FBS), the number of adhering cells has been found to correlate with the hydrophilicity and polarizability of the surface (Carré and Lacarriére, 2010). Intriguingly, the fraction of adhering cells increased to 90% or more in the absence of FBS (Carré and Lacarriére, 2010). This led to the suggestion that instead of focusing on the surface free energy or surface free energy components of the solid substrates, the focus should be on the interfacial free energy between the culture medium and the solid substrate (Carré and Lacarriére, 2010). Therefore, to be able to understand and model the role of surface energy in cell–substrate interactions, the composition of the liquid phase should be known.

Nevertheless, surface energy can have an effect on the later stages of bone formation and calcification by influencing the types of cells that initially attach themselves to the material and differentiate at the implant-cell interface. Hydrophilic surfaces may accelerate the early stages of the osseointegration of titanium implants by increasing osteoblast attachment to these types of surfaces *via* $\alpha_2\beta_1$ integrin-mediated binding and by promoting the secretion of Dkk2. Dkk2 acts upon distal MSCs by inducing osteoblastic differentiation (Olivares-Navarrete *et al.*, 2010) (explained in Section 2.2.5).

3.3 Surface topography

Surface roughness is the measure of the topographic relief of the surface. The most widely used parameter to quantify surface roughness is the arithmetic average of the absolute value of the profile from a midline, R_a, which can be determined using the following equation:

$$R_a = \frac{1}{lr}\int_0^{lr} |z(x)|dx, \tag{3.3}$$

where $z(x)$ is the absolute profile value from a midline and lr is the sampling length over which the surface profile has been measured (Tomlins *et al.*, 2005). However, the averaged R_a values lack detailed information about the geometry of the surface or the variations in peak heights or valley depths. Though different peak-valley parameters have been developed, the simplest approach is to determine the highest and lowest points within the overall measuring length. The R_{pv} (peak-to-valley roughness) value can be estimated as the vertical distance between the farthest points.

The effects of microtopography on cell behaviour have been studied extensively since 1964 when Curtis first proposed that cells react to their geometrical environment (Curtis and Varde, 1964). From randomly modified surfaces prepared using simple surface modification methods, such as mechanical polishing and sand-blasting, current research has advanced to the point of producing surface structures with nanometre resolution. High levels of resolution are desired because cells can react to topographical features as small as 5 nm (Curtis and Wilkinson, 2001), and even the conformation and symmetry of these nanofeatures can affect cellular behaviour (Dalby *et al.*, 2007).

Geometrically controlling the topography enables regulation of:

1. mechanical interlocking;
2. cell size and shape;
3. elongation and alignment of the nuclei (Brammer *et al.*, 2009);
4. integrin positioning and focal adhesion formation (Yim *et al.*, 2010; Cavalcanti-Adam *et al.*, 2007; Sjöström *et al.*, 2009);
5. cell–cell interactions;
6. the functional behaviour of proteins (Dalby *et al.*, 2006; Jedlicka *et al.*, 2007).

The mechanical interlocking theory of adhesion states that good adhesion occurs only when an adhesive penetrates the pores, holes and other irregularities of the adhered surface of a substrate and locks mechanically onto the substrate.

The relationship between the size/shape of the cell and its differentiation has been demonstrated by many different researchers. For example, large patterns (100 µm $\times$ 100 µm) promote osteogenesis, whereas small

patterns (32 µm × 32 µm) enhance adipogenesis (McBeath *et al.*, 2004). Furthermore, an angular star shape promotes osteogenesis, whereas a rounded flower shape with the same surface area results in adipogenesis (Kilian *et al.*, 2010). Generally speaking, a rounded cell shape supports cartilage formation (Zanetti and Solursh, 1984; McBride and Tate, 2008) and an adipogenic phenotype (McBeath *et al.*, 2004), whereas osteogenesis is promoted by the formation of cytoskeletal tension (Ruiz and Chen, 2008; McBeath *et al.*, 2004; Oh *et al.*, 2009; Kilian *et al.*, 2010). The size/shape effect activates RhoA and its effector ROCK kinase (McBeath *et al.*, 2004), as well as ERK, in conjunction with elevated Wnt signalling, which promotes osteogenesis (Kilian *et al.*, 2010).

Geometric patterning is useful for controlling the cell—cell interactions. This has been demonstrated with embryonic stem cells; the aggregation of embryonic stem cells into embryonic bodies can be spatially controlled using microtopography to facilitate a more homogeneous and controlled differentiation (Karp *et al.*, 2007). Bone formation starts when mesenchymal cells form local condensations in the form of cell clusters (Hall and Miyake, 2000). Controlling the cell—cell interactions with geometric patterning provides an interesting option for controlling osteogenesis.

3.4 Surface charge

According to electrostatic theory, an electrical double-layer is produced at any interface and the consequent electrostatic forces at the interface account for adhesion and resistance to separation. In the electrochemical double-layer model, the first layer consists of charge carriers that are adsorbed directly onto the object due to chemical interactions (a stationary layer). In the second layer, the charge carriers are attracted to the surface charge via the Coulumb force (a mobile layer) at a greater distance. The electric potential at the shear plane separating the stationary and mobile layers is called the ζ-potential (Fig. 3.2).

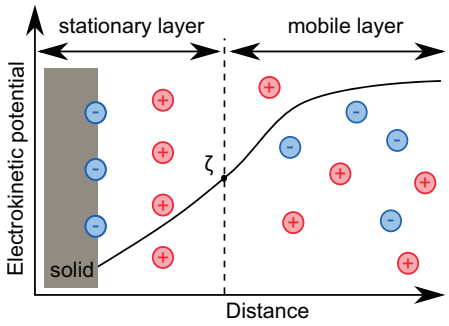

Figure 3.2. An electrochemical double layer is formed at the interface between a solid surface and the surrounding solution. The charge distribution is divided into a stationary and a mobile layer, which are separated by a shear plane. The zeta potential, ζ, is assigned to the potential decay at this shear plane.

The DLVO (named after Derjaguin & Landau and Verwey & Overbeek) theory was developed to explain the behaviour of non-living colloid suspensions. The interaction potential, V_{tot}, between micrometre-sized particles was calculated as the sum of two factors resulting from the van der Waals interactions (V_{vdW}, generally attractive) and repulsive Coulumb interactions (V_{dl}), which in turn result from the overlap between the electrical double-layer of the cell and the substrate:

$$V_{tot} = V_{vdW} + V_{dl}. \tag{3.4}$$

The cells have a diameter of several micrometres, they are surrounded by a hydrophobic plasma membrane that is expected to generate an electrodynamic attraction, and they bear a net negative surface charge. Therefore, the basic principles of DLVO theory should be applicable to cells.

Indeed, it has been demonstrated that cell-cell or cell-surface adhesion can be efficiently inhibited by electrostatic repulsion (Gingell and Todd, 1980) and that a van der Waals interaction between the biomimetic membranes exists (Yu *et al.*, 1998). However, no experimental work has resulted in a numerical determination of Hamaker constants (which represents the strength of van der Waals interactions between macroscopic objects) and surface charge densities that accurately accounts for the adhesive behaviour of precise cells and surfaces (Vitte *et al.*, 2004).

A major problem in applying DLVO theory to cells is that cells cannot be considered smooth structures when they are separated by a distance of less than 10 or 20 nm, which corresponds to the primary and secondary energy minimum in DLVO theory. For example, the length of integrins from the cell surface is approximately 23 nm (Komatsu *et al.*, 1997). Consequently, the precise distribution of charges on cell membrane molecules, as well as the shape of the cell surface at the submicrometre level, regulates cell–material interactions.

Nevertheless, the surface charge of the material influences the protein–material and cell–material interactions. Opposite charges between the substrate surface and protein promote protein adsorption, while the repulsion of like charges reduces protein adsorption. In general, ECM proteins have a negative charge and the cell membranes adhere closely to positively charged surfaces, whereas contact occurs only at distinct points on near-neutral and negatively charged surfaces (Davies *et al.*, 1986). Moreover, negatively charged surfaces show superior osteobonding activity compared to non-charged surfaces or positively charged surfaces

(Nakamura *et al.*, 2004). The explanation for this may be that the negative surface charge enhances calcium deposition on the surface.

3.5 Electrowetting

Electrowetting is the modification of the wetting properties of a surface with an applied electric field. This technique has recently gained a great deal of interest due to its potential to manipulate cell suspensions. The aim is to develop cell sorters for research and clinical diagnostics. Electrowetting can also be applied to implant materials. For example, the electric polarization of hydroxyapatite increased the hydrophilicity of the surface, which resulted in enhanced osteoblastic adhesion and spreading compared to normal hydroxyapatite (Nakamura *et al.*, 2009).

Some therapies that use electromagnetic fields are applied to improve the osseointegration of an implant. Therefore, the effect of electromagnetic fields on cell-material interactions, for example in the form of electrowetting, should be taken into consideration. Conversely, the effect of the surface on the electric field *in vivo* should be considered. Nonetheless, the typical range of electric fields used in the therapies (or induced by PEMF) are much lower (a few hundred mV/cm at most) (Hartig *et al.*, 2000; Chang *et al.*, 2004) than those applied for the manipulation of cells (a few kV/cm) (Zimmermann *et al.*, 2000; Fan *et al.*, 2008).

3.6 Conclusion about predicting cellular responses to material

The cell–surface interaction involves three phases: protein adsorption, cell adhesion and cell activation. Of these, not even the first phase can easily be predicted. The question has not only to do with which proteins adsorb on the surface and which have the largest affinity to the surface, but also with what kinds of conformational changes may occur upon adsorption and how that affects the functionality of the proteins. Second, cell adhesion on the substrate cannot be determined solely by the non-specific physical interactions because of the specific ligand recognition, which the simple models do not take into account. Third, it is not yet completely understood how cell adhesion and the activation of the adhesion molecules regulate the subsequent cellular responses. For example, as explained in Section 2.2, the process of osteogenic differentiation has only recently become understood.

4. Pulsed Electromagnetic Fields and Osteogenesis

Pulsed electromagnetic fields (PEMF) accelerate the healing process if applied across the site of a bone fracture (Bassett *et al.*, 1974). PEMF therapy has been clinically used since it was first approved by the Food and Drug Administration in 1979. It has been used, for example, to treat osteoporosis (Tabrah *et al.*, 1990; Rubin *et al.*, 1989), bone fracture (Griffin *et al.*, 2008) and implant osseointegration (Dimitriou and Babis, 2007).

Still, after 40 years of research, the cellular and molecular mechanisms by which the PEMF exerts its effects are not understood. Whereas PEMF might affect, for example, the electrostatic adhesion of cells, no effects on the cell adhesion molecules (integrin, CD44) were observed (Zhang *et al.*, 2011). Recently, it has been proposed that PEMF can modulate calcium-binding to calcium-modulated protein (calmodulin) (Pilla *et al.*, 2011). Calcium/calmodulin then activates a nitric-oxide synthesis that coordinates the release of cytokines and growth factors (Diniz *et al.*, 2002b; Pilla *et al.*, 2011). Although osteoprogenitor cells play a key role in bone healing, the direct effect of PEMF on them has been poorly studied.

Table 4.1 summarises previous studies on the effect of PEMF on osteoblasts or MSCs. PEMF-induced osteogenesis has been shown to be dependent on the intensity and pulse duration of the stimulation: the pulse durations of 25 and 50 µs increased ALP activity more than pulse durations of 6, 12 or 100 µs and magnetic intensities of 0.04–0.4 mT enhanced bone formation more effectively than intensities of 0.01–0.02 or 0.6–0.8 mT (Matsunaga *et al.*, 1996). The different types of stimulation can explain the majority of the apparently inconsistent results presented in Table 4.1. Nonetheless, the type of PEMF stimulus being used varied too greatly to enable us to draw unambiguous conclusions about the optimal stimulation. Furthermore, Publication V showed that the type of stimulus is not the only parameter that explains the inconsequent results. The results described in Section 9.4.1 were different from those

obtained by Jansen *et al.* (2010), despite the fact that we used the same stimulus. This inconsistency can be explained by the difference in the cell density, which is critically important for the lineage-specific differentiation of MSCs *in vitro* (Pittenger *et al.*, 1999; McBeath *et al.*, 2004). With increasing density, the adhesion and spreading of cells against the substrate decrease, while cell-cell contact and paracrine signalling increase. In addition, plating density alters cell shape, which provides an important cue that regulates an adipogenic-osteogenic switch in MSC lineage commitment (McBeath *et al.*, 2004).

Table 4.1. Previous PEMF research with osteoblastic cells and MSCs related to proliferation and/or osteogenic differentiation. The up arrow (↑) specifies an up-regulated effect and the down arrow (↓) a down-regulated effect, respectively. Here 'differentiation' refers to osteogenic differentiation. The saturation density of MSCs and osteoblasts is approximately 10 000 cells/cm^2, while osteosarcoma cell lines have 15 to 20-fold higher saturation densities (Pautke *et al.*, 2004).

Cells, density	**PEFM type**	**Effects on cells**	
MG63	1.8 mT, 15 Hz, 5 ms bursts	↓ proliferation	[1]
confluence	of 20 pulses	↑ differentiation (ALP, OC)	
MCT3T3-E1	7 mT, 15 Hz, 5 ms bursts of	↑ proliferation	[2]
7800 cells/cm^2	150 µs square waves	↑ differentiation (ALP)	
Mouse calvarial	0.1 mT, 15 Hz, 5 ms bursts	↑ proliferation	[3]
10000 cells/cm^2	with 0.2 ms pulses, 8 h/day	↓ differentiation (ALP)	
MCT3T3-E1,	2.4 mT, 1.8 mT or 0.09 mT,	↓ mature α1(I) collagen	[4]
NHO, CTP-BM	67.1 ms bursts with 21, 98		
30000 cells/cm^2	or 1619 pulses		
MG63, SaOS-2,	1.6 mT, 15 Hz, 4.5 ms	↓ SaOS-2 proliferation on CaP	[5]
NHO confluent	bursts of 20 pulses, 8 h/day	↑ differentiation (OPG)	
hMSC 1000 and	1.8 mT, 15 Hz, 4.5 ms	↑ proliferation	[6]
5000 cells/cm^2	bursts of 20 pulses, 8 h/day		
hMSC 1500 and	0.13 mT, 7.5 Hz, 300 µs	no effect on proliferation	[7]
3000 cells/cm^2	pulses, 2 h/day	↑ differentiation (ALP, RUNX2)	
hMSC	0.1 mT, 15 Hz, 5 ms bursts	↓ proliferation	[8]
10500 cells/cm^2	with µs pulses, continuous	↑ differentiation (BMP2, OC, BSP)	
Rat MSC	1 mT, 15 Hz, 66 mS, conti-	↑ differentiation (RUNX2, ALP,	[9]
10500 cells/cm^2	nous	BMP2, BSP)	
hMSC	1.6 mT, 15 Hz, 4.5 ms	↑ osteogenic effects of BMP2	[10]
confluent	bursts of 20 pulses, 8 h/day	(OPG)	[11]

[1] Lohmann *et al.* (2000); [2] Diniz *et al.* (2002a); [3] Chang *et al.* (2004); [4] Sakai *et al.* (2006); [5] Schwartz *et al.* (2009); [6] Sun *et al.* (2009); [7] Tsai *et al.* (2009); [8] Jansen *et al.* (2010); [9] Yang *et al.* (2010); [10] Schwartz *et al.* (2008); [11] Schwartz *et al.* (2009); CTP-BM = human connective tissue progenitor cells from bone marrow; hMSC = human MSC; MCT3T3-E1 = mouse osteoblastic cell; MG63 = human osteosarcoma cell; NHO = normal human osteoblasts; SaOS-2 = human osteosarcoma cell.

5. Dehydroepiandrosterone and Osteogenesis

Dehydroepiandrosterone (DHEA) is a pro-hormone produced in the reticular zone of the adrenal cortex, but only in human beings and other primates. After cellular intake, it can be metabolised by steroidogenic, intracrine enzymes into various active sex steroids, *e.g.* estradiol (E2) or dihydrotestosterone (DHT) (Fig. 5.1). Researchers have long believed that such functionally active estrogens and androgens play a key role in bone metabolism, and their failure is a well-recognised cause of postmenopausal osteoporosis in women and osteoporosis in male hypogonadism (Khosla *et al.*, 2008; Slemenda *et al.*, 1987). Furthermore, androgens may promote preosteoblastic differentiation via effects on the canonical Wnt signalling pathway (Liu *et al.*, 2007).

In rodents, DHEA protects against osteoporosis (Canning *et al.*, 2000; Clerici *et al.*, 1997; Harding *et al.*, 2006), and promotes osteoblast growth and affects the quality of the bone tissue that forms (Wang *et al.*, 2007). Nonetheless, in human patients treated with glucocorticoids (a common side effect of which is steroid-induced osteoporosis), DHEA provided only a moderate increase in the density of the bone mineral (Bovenberg *et al.*, 2005; Hartkamp *et al.*, 2004; von Mühlen *et al.*, 2008). Species-specific differences in the adrenal and intracrine metabolome exist and may explain the lack of translation between species. DHEA is abundant in human circulation, while it is very low or absent in rodents (Wolf and Kirschbaum, 1999), and exogenous DHEA in rodents is efficiently converted into highly oxidized metabolites (Marwah *et al.*, 2002). Many of the functions initially attributed to DHEA in rodents are now thought to be due to these oxygenated metabolites. In humans, many of the actions of DHEA are presumably mediated through its conversion into sex hormones.

MSCs contain some of the essential intracrine enzymes, namely 3β-hydroxysteroid dehydrogenase (HSD) and 5α-reductase. Furthermore,

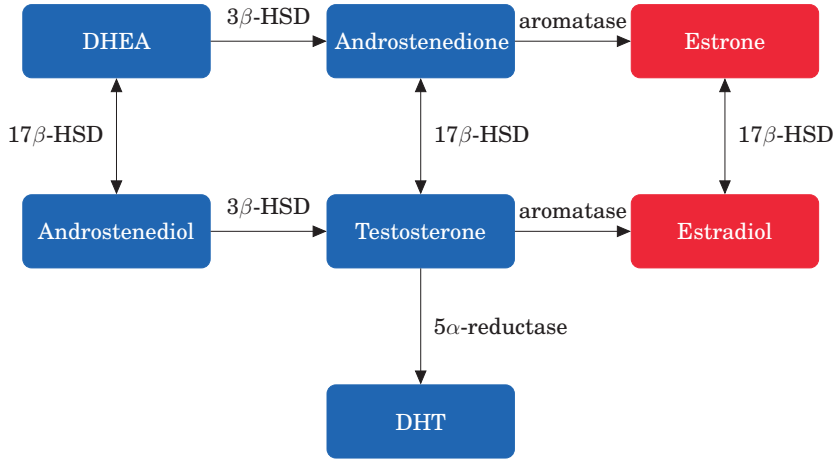

Figure 5.1. Intracrine conversion of dehydroepiandrosterone (DHEA) into dihydrotestosterone (DHT). The enzymes involved are 3β-hydroxysteroid dehydrogenase (HSD), 17β-HSD and 5α-reductase. These reactions are unidirectional, except for the 17β-HSD catalysed reaction, which can run in both forward and reverse directions in an enzyme isoform-dependent manner. In addition, many of the undirectional enzymes comprise several different isoforms, which probably enable cell- and situation-specific regulation and steroidogenic tailoring. The androgens are the blue rectangles and the estrogens are the red rectangles.

in the presence of DHEA, the intrinsic 'bridging' enzyme 17β-HSD is induced (Sillat *et al.*, 2009). This should make DHEA-to-DHT conversion in MSCs possible (Fig 5.1). This conversion can be blocked by inhibiting 5α-reductase, which is the enzyme catalysing the final reaction in the DHEA-to-DHT pathway, converting testosterone into DHT. Futasteride and dutasteride are 5α-reductase inhibitors. Dutasteride inhibits both the type I and type II forms of 5α-reductase; therefore, it is more effective in this respect than futasteride, which inhibits the type II form of the enzyme only.

Research on the effect of DHEA on human MSCs has mainly focused on neurogenic differentiation (Shiri *et al.*, 2009), and there were no previous reports related to the eventual effect of DHEA on the osteogenic differentiation of human MSCs.

6. Bacterial Infection

Bacterial adhesion is equally complicated as cell adhesion and it is influenced by many factors, including bacterial properties, material surface characteristics and environmental factors, such as the presence of serum proteins and flow conditions. Cytocompatible surfaces may also offer a favourable platform for adhesion, growth and the biofilm formation of microbes. Besides the effect of directly anti-bacterial materials, little is known about how material properties influence bacterial adhesion. However, it seems that bacterial adherence depends primarily on the infective microorganism and on the response of each individual patient rather than on the materials or components (Gómez-Barrena *et al.*, 2012).

Interestingly, the number of adherent bacteria correlates negatively with the amount of adsorbed proteins on nanostructured samples. The accumulation of proteins on rough surfaces downplays bacterial adhesion and biofilm formation by creating a thick layer that reduces the more direct interaction of bacteria with the nanostructured surface, thereby inhibiting bacterial adhesion (passivation effect). Moreover, the protein layer significantly flattens the surface, suppressing the area of the nanoscale surface available for bacterial adhesion (flattening effect).

Bacterial infections remain a common cause for why many types of implants ultimately fail (Darouiche, 2004, 2001). In all but the most nutrient-rich environments, bacteria grow preferentially in extracellular polymeric substance- (bacterial-slime) enclosed communities that are attached to surfaces, *i.e.* as biofilms. The presence of these microbial biofilms always triggers pathogenic changes in the surrounding tissues, but the symptoms in such indolent biofilm-associated infections develop often slowly. The infected abiotic and immune-compromised implant surfaces and materials act as bacterial growth substrates and reservoirs, impairing implant function and propagating the local spreading of the infection into surrounding

tissues and hematogenic metastatic infections into distant sites. Recognising the colonisation of the implant surface by bacteria remains an important clinical and academic issue.

Recognition of the differences between planktonic and biofilm bacteria has disclosed many important differences of relevance between these two microbial states (Costerton *et al.*, 1978, 1999). Biofilm bacteria are not easily accessible to naive and immune host defence cells or soluble factors, such as complement or antibiotics. Furthermore, dormant pathogens embedded in the biofilm and adhering to the implant surface can be difficult to detach and grow in a bacterial culture. Therefore, different approaches have been developed to diminish false negative culture results, *e.g.* multiple sampling from the surface of the implant (direct swabs) and sonication of the implant to detach and disperse bacteria and biofilms from the implant surface to culture medium (Marculescu *et al.*, 2005; Neut *et al.*, 2003; Panousis *et al.*, 2005; Trampuz and Widmer, 2006; Trampuz and Zimmerli, 2006; Zimmerli, 2006). These studies have confirmed that bacteria are present in many cases that were previously considered culture-negative cases. This led to the suggestion that at least some cases of failed orthopaedic implants that were considered to represent aseptic loosening (based on the absence of clinical signs of infection and the failure to isolate and culture bacteria) may actually have an infectious etiology (Nelson *et al.*, 2005). Unfortunately, none of these methods is perfect and the frequent use of antibiotics before collecting the sample further increases the risk of false-negative culture results. However, false-positive culture results are also possible, usually as a result of contamination during sample processing and culture.

7. Aims of the Study

The main aim of this study was to find methods that could potentially improve the osseointegration of an implant.

I The first aim was to investigate whether the surface micro-patterning could enhance the cytocompatibility of the cell-unfriendly, silicon-based implants and improve their biocombatibility during the initial phase of osseointegration, *i.e* osteoblastic and progenitor cell adhesion and the osteogenesis of MSCs.

II The second aim was to broaden the study from two-dimensional patterns to three-dimensional patterns and to examine its effect on osteoblastic, fibroblast and MSC adhesion and the osteogenesis of MSCs.

III Since other external factors can also regulate osseointegration, the third aim was to investigate the effect of PEMF and DHEA on osteoblastic cell and MSC proliferation and the ostegenic differentiation of MSCs.

IV In addition to osseointegration, another important factor determining the lifetime of an implant is the bacterial adhesion on its surfaces, which can cause infection and septic loosening of the implant. Diagnosing bacterial infection is challenging, and therefore the fourth aim was to test the potential of novel spectroscopic methods to recognise bacterial implant infections.

8. Materials and Methods

Table 8.1 summarises the materials and methods utilised in this thesis.

Table 8.1. Summary of the materials and methods used in the present thesis.

Study	Substrate / stimulus	Characterisation	Cells	Testing methods
I	Patterned substrates (Fig. 8.1 A–C) of DLC, Cr*, Ta* and Ti		SaOS-2	SEM, IHC
II	Patterned (Fig. 8.1 C and D*) and planar substrates of DLC, Cr, Ta and Ti	Roughness and contact angle measurements	MSC	SEM, IHC
III	Patterned (Fig. 8.1 C and D) and planar substrates of DLC, Cr, Ta and Ti	ζ-potential measurements	MSC	qRT-PCR, colorimetry
IV	3-D (Fig. 8.1 E and F) of Si, TiO_2, DLC and Ormocomp®		SaOS-2, fibroblasts, MSC	SEM, IHC
V	PEMF and DHEA		SaOS-2, MSC	qRT-PCR, IHC colorimetry
VI	Patterned (Fig. 8.1 C) and planar substrates of DLC and Ti		MSC, *S. aureus*, co-cultures	SEM, XPS, ToF-SIMS

* Additional materials not included in the original publications.

DLC = diamond-like carbon; IHC = immunohistochemistry; qRT-PCR = quantitative real-time polymerase chain reaction; SEM = scanning electron microscopy; ToF-SIMS = time-of-flight secondary ion mass spectrometry, XPS = X-ray photoelectron spectroscopy.

8.1 Substrate fabrication (I–IV,VI)

A wide variety of microfabrication techniques and materials were used in this thesis study. A description of the samples and the fabrication processes is given in this section.

The size of all the substrates was 10 mm $\times$ 10 mm. In the first set of substrates (I), each substrate consisted of four quadrants. Three of the

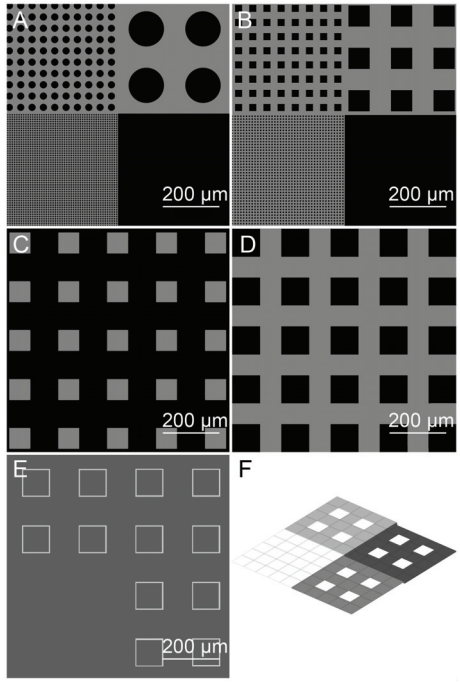

Figure 8.1. A schema presenting the substrate types. The first substrate set consists of panels A and B. Here, the dark areas represent DLC, Cr, Ta or Ti patterns on a Si background, or alternatively, inverse substrate-type Si patterns on a coated background. For the second substrate set, panel C is a square-patterned substrate and panel D is an inverse square-patterned substrate. The dark colour represents Si and the light colour represents the coating (DLC, Cr, Ta or Ti). For the third substrate set, panel E shows the location of the pillars and panel F shows the height differences between the 3D-substrates. Here, the surface was either Si, TiO_2, DLC or Ormocomp®.

quadrants contained squares with the length of the sides being 5, 25 or 125 µm or circles with diameters of 5, 25 or 125 µm; they were coated with diamond-like carbon (DLC), Cr, Ta or Ti on a Si background (Fig. 8.1 A, B). Regardless of the size of the pattern, the circles covered 30.6% and the squares covered 25% of the surface. The fourth quadrant contained a homogeneous coating as a control. In addition, an inverse version of these substrates was fabricated, *i.e.* uncoated Si squares or circles on a background coated with DLC, Cr, Ta or Ti.

The second set of substrates (I–III, VI) contained regularly spaced, 75 µm × 75 µm squares coated with DLC, Cr, Ta or Ti at a distance of 100 µm (Fig. 8.1 C). An inverted version of these samples contained 100 µm × 100 µm Si-squares at a distance of 75 µm on a background coated with DLC, Cr, Ta or Ti (Fig. 8.1 D). In the second set of substrates, the coating occupied 18.4% or 67.3% of the surface, respectively. In addition, the planar control substrates were coated with DLC, Cr, Ta and Ti.

In the third set of substrates (IV), each chip was also divided into four parts: one part was a planar control surface and the other three parts contained 100 µm × 100 µm squares of square pillars of different heights (200 nm, 5 µm or 20 µm) at a distance of 100 µm (Fig. 8.1 E, F). The surface was either Si, TiO_2, DLC or Ormocomp®.

Based on the results, the square patterns had a stronger impact on the cytoskeletal organisation than the circular patterns. Since it is known that activation of the cytoskeleton enhances osteogenesis, the square patterns were selected for the studies focusing on the osteogenesis of MSCs.

8.1.1 Patterned surfaces (I–III, VI)

Polished <100> Si wafers (p-type) were dry-baked with an adhesion promoter (20% hexamethyldisilazane in xylene). Then, the chosen photoresist was applied for patterning and cured using optimised process parameters. DLC was deposited using a filtered pulsed plasma arc discharge (FPAD) or laser ablation and Cr, Ta or Ti coatings were magnetron sputtered onto the surface of the resist-patterned wafers. The process parameters were optimised to achieve well–adhering, smooth coatings with a thickness of 200 nm. The micro-patterns were revealed via a lift-off procedure by immersing the wafers in a resist remover in an ultrasonic bath.

8.1.2 Fabrication of three-dimensional surfaces (IV)

3D Si substrates were fabricated using ultraviolet lithography and plasma etching. Three masks, one for each pillar height, were used. Reactive ion etching was applied to produce the lowest 200 nm pillars and anisotropic deep reactive ion etching was applied to produce the 5 µm and 20 µm pillars. Some of the Si substrates were coated either with TiO_2 using an atomic layer deposition or with DLC using the FPAD method, whereas the reference substrates were left uncoated. The Ormocomp® (Micro Resist Technology, Berlin, Germany) pillars were fabricated using ultraviolet embossing and a plasma treatment.

8.2 Substrate characterisation (II, VI)

Contact angle measurements, atomic force microscopy and ζ-potential measurements were used in this thesis for the quality controls and for characterising the planar and micro-patterned substrates. Brief descrip-

tions of these techniques are given in this section (8.2).

8.2.1 Contact angle and surface energy measurements (II)

The contact angle measurements were performed to clarify the wettability of the materials studied. The contact angle of the sessile drops (15 µl) were measured using a custom-made apparatus (an optical SZ-PT Olympus microscope equipped with a C-3030ZOOM digital camera; Olympus Corp., Tokyo, Japan). To assess the total surface energy and its polar and dispersive components, the contact angles for water (polar) and diiodomethane (non-polar) were measured. Gnu Image Manipulation Program (GIMP, www.gimp.org) image analysis software was used to determine the contact angles for left and right margins. Five parallel samples were examined and the dispersive and polar components were calculated using the Owens-Wendt model:

$$(1 + \cos\theta)\gamma_L = 2((\gamma_S^D \gamma_L^D)^{1/2} + (\gamma_S^P \gamma_L^P)^{1/2}) \quad (8.1)$$

where θ is the measured (averaged) contact angle value, γ is the surface tension, the superscripts D and P label the dispersive and polar component of the surface tension, respectively, and the subscripts S and L stand for solid and liquid, respectively (Owens and Wendt, 1969). The total surface energy (γ_S) is the sum of the dispersive and polar components.

8.2.2 Roughness measurements (II)

An atomic force microscope (PSIA XE-100; Park Systems Corp., Suwon, Korea) was used to analyse the topography of the substrates and to determine the thickness of the thin film depositions. Aluminium-coated silicon cantilevers (Acta-10, ST Instruments B.V., LE Groot-Ammers, The Netherlands) were used in a non-contact mode to scan the surface across an area of 2 µm $\times$ 2 µm with a scanning rate of 0.25 Hz. The average surface roughness (R_a) and peak-to-valley roughness (R_{pv}) were determined from six random locations using instrument analysis software (XIA).

8.2.3 ζ-potential measurements (III, VI)

A streaming current measurement was used to examine the interface charges of the studied solid biomaterials immersed in a liquid. The ζ-potentials of the surfaces were measured for two pairs of each substrate type in 1 mM of KCl (pH 7) using the adjustable gap cell of an elec-

trokinetic analyser for the solid substrates (SurPASS, Anton Paar GmbH, Austria). Each measurement was repeated three times. The ζ-potential was calculated from the streaming current measurements according to the Helmholtz-Smoluchowski equation (Lyklema, 1995):

$$\zeta = \frac{dI}{dP} \times \frac{\eta}{\epsilon \times \epsilon_0} \times \frac{L}{A} \tag{8.2}$$

where ζ is the ζ-potential, $\frac{dI}{dP}$ is the slope of the streaming current vs. pressure, η is the electrolyte viscosity, ϵ is the permittivity, ϵ_0 is the dielectric coefficient of electrolyte and L is the length and A the cross section of the streaming channel.

8.3 Cell cultures (I–VI)

Publications I−IV investigated the cellular responses to the biomaterial substrates, Publication V investigated the effect of PEMF and DHEA on osteoblast-like cells and osteogenesis and Publication VI investigated the footprint that cells produce and leave after detachment on the surface as a cellular imprint. This section (8.3) describes the cell culture methods used in the above-mentioned studies.

The cells were cultured at 37 °C in a humidified atmosphere containing 5% CO_2. All substrates were cleaned in 70% ethanol and sterilised using 30 kGy gamma irradiation prior to being exposed to the cells.

8.3.1 Osteoblastic SaOS-2 cultures (I, IV, V)

The adhesion of human osteogenic sarcoma (SaOS-2, ECACC 890500205) cells on patterned surfaces (I) and on 3D surfaces (IV), as well as the effect of PEMF and DHEA on the proliferation of SaOS-2 cells, was studied (V). SaOS-2 cells were cultured in McCoy's 5A medium containing GlutaMAX$^{\mathrm{TM}}$ (Gibco/Life Technologies Inc., Gaithersburg, MD, USA) and supplemented with 10% FBS, 100 IU/ml penicillin and 100 µg/ml streptomycin. The SaOS-2 cells were seeded onto the substrates at a density of 25×10^3 cells/cm^2 and cultured for 48 h (I, IV) or for 4−14 d (V).

8.3.2 Mesenchymal stem cell cultures (II–V)

The adhesion and osteogenic differentiation of MSCs was studied on micropatterned and 3D surfaces (II−IV) and the effect of PEMF and DHEA on the proliferation and osteogenic differentiation of MSCs was evaluated

(V). Finally, the footprint that MSCs produce and leave on the surface was compared to the footprint of *S. aureus* (VI).

Human bone marrow-derived MSCs (4−6th passage, Poietics^{TM}, Lonza, Basel, Switzerland) were cultured using a Lonza Mesenchymal Stem Cell Basal Medium with a Mesenchymal Cell Growth Supplement (MSCGM), L-glutamine and GA-1000 (Gentamicin / Amphotericin-B) or penicillin-streptomycin. For the adhesion experiments, the cells were seeded onto the surfaces at a density of 0.5×10^4 cells/cm^2 and cultured for 7.5 h, 120 h (80% confluence) or up to 28 d (proliferation experiment). For the osteogenic experiments, the cells were seeded at a density of 0.3×10^4 cells/cm^2 and cultured for up to 28 d. Osteogenesis was induced 24 h after seeding by replacing the MSCGM with the Osteogenesis Induction Medium (which contained ascorbate, β-glycerophosphate and dexamethasone, penicillin-streptomycin, a growth supplement and L-glutamine, Lonza). The MSCs were fed every 3−4 d with the appropriate media.

8.3.3 Setting up the fibroblast cell line and cell culture (IV)

The effect of 3D surfaces on fibroblast adhesion was studied. Fibroblasts were isolated from a fibrous capsule sample collected from a 65-year-old male patient during joint replacement surgery. Fat and loose connective tissues were removed and the tissue was minced to pieces. The pieces were left overnight in an RPMI medium containing 10% FBS and 1000 IU/ml penicillin and 1000 µg/ml streptomycin. On the second day, the medium was changed to one with a 1:10 reduced penicillin/streptomycin concentration. The medium was changed twice a week, and at 80% confluence the tissue explants were removed and the cells were allowed to grow to confluence. For the experiment, 4th-passage fibroblasts were seeded onto the biomaterial surfaces at a density of 10^4 cells/cm^2 and cultured for 120 h (80% confluence) in D-MEM with GlutaMAX^{TM} (Gibco).

8.3.4 PEMF and DHEA stimulation (V)

The effects of PEMF and DHEA on the proliferation of SaOS-2 cells and MSCs and the osteogenic differentiation of MSCs were studied. Continuous PEMF stimulation was produced using an OSSATEC® Bone growth stimulation device (Fig. 8.2; Uden, The Netherlands); the device produced a 15 Hz, 0.1 mT EM field consisting of 5 ms bursts with 1 µs pulses.

The cells were cultured in the presence of 100 µM, 10 µM or 1 µM DHEA

(Sigma, St. Louis, MO, USA) with and without the presence of 100 nM dutasteride (Avodart®, GlaxoSmithKline, Middlesex, UK), which inhibits types I and II 5-α-reductase.

The stimulation was started 24 h after seeding. The cells were grown on 24-well plates (proliferation experiments), 12-well plates (gene expression) or 8-well chamber slides (staining).

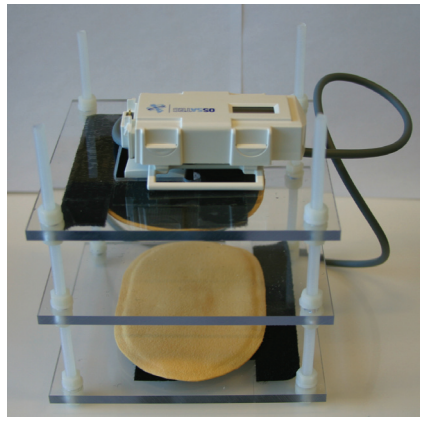

Figure 8.2. The set-up of the pulsed electromagnetic field device. The cell culture plate is placed between the coils, which are inside the yellow pads. The distance from the cells to both of the coils is of an equal length.

8.3.5 *Staphylococcus aureus* cultures (VI)

The MSC footprint was compared to *S. aureus* footprint. A biofilm producing strain of *S. aureus* S-15981 (Valle *et al.*, 2003) was cultured at 37 °C. Pre-experiment cultures were conducted in a tryptic soy broth (TSB) until a stationary phase of growth was achieved. For the experiment, the concentration was adjusted to 6×10^8 colony forming units (CFU)/ml. The samples were incubated for 48 h at 37 °C. They were gently rocked continuously and refreshed once during the incubation.

8.3.6 Co-culture of *S. aureus* and mesenchymal stem cells (VI)

Two types of MSC and *S. aureus* co-cultures were prepared in MSCGM without antibiotics to further compare the footprints of these cells. In the first set-up, the MSCs were seeded on the substrates at a density of 6000 cells/cm^2 and cultured for 48 h; this was followed by the addition of a S-15981 staphylococcus solution (6×10^8 CFU/ml) and incubation for another 48 h. In the second set-up, MSCs and S-15981 were incubated simultaneously for 96 h using the above-mentioned seeding density and concentration. The viability of bacteria in MSCGM was examined using a Live/Dead BacLight kit, while the viability of MSC in the co-cultures was examined using a Live/Dead Kit for mammalian cells (Molecular Probes / Life technologies). To assess the amount of biomass in a biofilm, crystal violet staining was applied.

Table 8.2. Sequences of the primers used in a qRT-PCR reaction.

Gene		Sequence	Amp. size (bp)
COLα1 (I)	5'	CCACCAATCACCTGCGTACAGAA	118
NM 000088.3	3'	GGGCAGTTCTTGGTCTCGTCACA	
RUNX2	5'	TAGATGGACCTCGGGAACCCAGA	309
NM 001024630.2	3'	TGGAAGACAGCGGGGTGGTAGA	
ALP	5'	CTTGACCTCCTCGGAAGACACTC	237
NM 000478.3	3'	GCCTGGTAGTTGTTGTGAGCATAG	
SMAD1	5'	CCGTTTCCTCACTCTCCCAATAGC	245
NM 0001003688.1	3'	GCAACCGCCTGAACATCTCCTC	
OP	5'	CACAGCATCGTCGGGACCAG	250
NM 000582.2	3'	GGGCTAGGAGATTCTGCTTCTGAG	
OC	5'	CCTCACACTCCTCGCCCTATTG	112
NM 199173.3	3'	CGCTGCCCTCCTGCTTGG	
RPLP0	5'	GGCGACCTGGAAGTCCAACT	149
NM 001002	3'	CCATCAGCACCACAGCCTTC	
β-actin	5'	ATCACCATTGGCAATGAGCGGT	333
NM 001101.3	3'	TCTTCATTGTGCTGGGTGCCAG	

8.4 Evaluation of cell adhesion and osteogenic differentiation (I–V)

This section (8.4) describes the methods used in the evaluation of cell adhesion and osteogenic differentiation. Adhesion was studied using a scanning electron microscope (SEM) and actin-vinculin-nuclei staining. Osteogenic markers were stained and measured colorimetrically and/or with a quantitative real-time polymerase chain reaction (qRT-PCR) (II−V).

8.4.1 Scanning electron microscopy of cells (I, II, IV)

Subsequent to the incubation, the samples were washed in a phosphate buffered saline (PBS), fixed in 2.5% glutaraldehyde (Sigma) overnight at 4 °C, washed in PBS and dehydrated in the ethanol series. The dehydration was completed using a Bal-Tec CPD 030 Critical Point Dryer (BAL-TEC AG, Balzers, Liechtenstein). The samples were mounted on SEM stubs, coated with Pt using an Agar sputter device (AGAR, Stansted, England) and examined using a Zeiss DSM 962 SEM (Carl Zeiss, Oberkochen, Germany) at an accelerating voltage of 8−10 kV.

The density, coverage and size of the cells on the patterns and on the background were calculated from the images that were segmented using Canny's edge detection algorithm (Matlab, MathWorks, Inc., Natick, MA). Three to four parallel samples were analysed and four images were taken from each sample.

8.4.2 RNA expression (III, V)

The RNA levels of six osteogenic markers (COLα1, RUNX2, ALP, SMAD1, OP and OC) were measured. Ribosomal protein large P0 (RPLP0) and β-actin were used as housekeeping genes. Total RNA was extracted using an RNeasy Mini Kit (Qiagen Valencia, CA, USA). Complementary first strand DNA (cDNA) was synthesized from 30 ng (III) or 100 ng (V) of total RNA using an iScript cDNA Synthesis Kit (Bio-Rad, Hercules, CA, USA). 2 µl of cDNA, 10 µl of IQ SYBR Green Supermix (Bio-RAD) and primers (Table 8.2) at a final concentration of 100 nM were used in the qRT-PCR, which was performed using an iQ5 real-time PCR detection system (Bio-Rad). The results were analysed using the comparative C_t method.

8.4.3 Immunohistochemistry (I, II, IV)

To study the adhesion of the cells, vinculin and actin cytoskeleton were stained (I, II, IV). To examine the signalling routes of osteogenesis, ERK and ROCK were stained (IV). To study osteogenesis, osteocalcin and/or osteopontin were stained (III, IV, V).

For immunohistochemistry, the samples were fixed in 4% paraformaldehyde (PFA) in PBS and permeabilized in 0.1% Triton X-100 in PBS. Non-specific binding sites were blocked using normal serum from the host species of the secondary antibody diluted at a ratio of 1:10 in 0.1% BSA in PBS. After blotting away the normal serum, the samples were incubated in primary antibodies (Table 8.3) for 1 h at 22 °C or overnight at 4 °C. The samples were incubated in secondary antibodies for 1 h at 22 °C. In vinculin and osteocalcin staining (in Publication II), Phalloidin-568 (1:30 in BSA-PBS) was incubated together with a secondary antibody to stain the actin cytoskeleton. The nuclei were stained with DAPI (4',6-diamidino-2-phenylindole). Washes were performed after all of the steps, except the blocking step.

8.4.4 Alkaline phosphatase (II–IV, V)

ALP is an early marker of bone formation. ALP activity was studied using a Naphthol-AS-MX phosphate sodium salt substrate at 14 d (Sigma, 1 g/l) and Fast red TR chromogen (Sigma, 1 g/l) in a 0.1 M Tris buffer (pH 8). Subsequent to a 1 h incubation, the samples were fixed in 4% PFA, permeabilized in 0.1% Triton X-100 in PBS and counterstained in DAPI.

Table 8.3. Antibodies used in immunohistochemistry.

Vinculin (I,II)
Monoclonal mouse anti-human vinculin IgG (Lehto and Virtanen, 1985)
Alexa-Fluor 488 conjugated goat anti-mouse IgG (Molecular Probes; 20 µg/ml)
ERK (IV)
Monoclonal mouse anti-human ERK IgG (Abcam; 1 µg/ml)
Alexa-Fluor 586 conjugated goat anti-mouse IgG (Molecular Probes; 20 µg/ml)
ROCK (IV)
Monoclonal rabbit anti-human ROCK-1 IgG (Millipore; 1:50)
Alexa-Fluor 488 conjugated goat anti-rabbit IgG (Molecular Probes; 20 µg/ml)
Osteopontin (IV, V)
Monoclonal mouse anti-human osteopontin IgG (Santa Cruz; 2 µg/ml)
Alexa-Fluor 568-conjugated goat anti-mouse IgG (Molecular Probes; 20 µg/ml)
Osteocalcin (II, V)
Polyclonal rabbit anti-human osteocalcin IgG (AbD Serotec 7060-1515; 1:40)
Alexa-Fluor 488-conjugated donkey/goat anti-rabbit IgG (Molecular Probes; 20 µg/ml)

Washes in the PBS were performed between all of the steps.

The ALP activity was quantified using SIGMAFAST p-Nitrophenyl phosphate tablets (III). The cells were lysed in a Passive Lysis Buffer (Promega, Madison, WI, USA), after which 200 µl of the stain-solution was incubated with supernatants for 30 min in the dark. The absorbance at 405 nm was measured using a Multiskan Ex-Photometric plate reader (Labsystems, Thermo Fisher Scientific, Finland). The analysis was done in triplicate.

8.4.5 MTT assay (V)

MTT (3-(4,5-Dimethylthiazol-2-yl)-2,5-diphenyltetrazolium bromide) is a yellow tetrazole that is reduced to a purple formazan in living cells and used to evaluate the proliferation rate of cells. MTT was used at a concentration of 1 mM for 2 (MSCs) or 3 h (SaOS-2 cells) at 37 °C. A solubilisation solution (10% sodium dodecyl sulfate in 1 mM HCl) was added to dissolve the insoluble purple formazan product into a coloured solution. Subsequent to the 17 h incubation, the absorbance at 570 nm was quantified using a Multiskan Ex-Photometric plate reader.

8.4.6 Mineralisation (II, IV)

Mineralisation was analysed using Alizarin Red S (II, IV) and hydroxyapatite-specific OsteoImage^{TM} staining (III, IV). For both protocols, the samples were fixed in 4% PFA. Alizarin Red S (2% in dH_2O, Sigma) was applied for 2 min; after this, the samples were rinsed in acetone, acetone-

xylene (1:1) and xylene. OsteoImage™ Mineralisation Assay (Lonza) was used according to the manufacturer's instructions and the mineral deposits were measured using a Plate CHAMELEON V plate reader (Chameleon Systems, Ruislip, UK; 485 nm for excitation and 535 nm for emission). Subsequent to the measurement, the actin cytoskeleton and nuclei were stained (Section 8.4.3).

8.4.7 Optical microscopy (I–V)

The stained samples were mounted in a mounting medium, coverslipped and examined using a Leica TCS SP2 confocal microscope (Werzlan, Germany), a Leitz Diaplan microscope (Wetzlar, Germany), an Olympus fluorescence microscope or a Leica DM6000 B/M microscope.

8.5 Footprint analysis (VI)

This section (8.5) presents the methods used to compare the MSC and *S. aureus* footprints. The cells and bacteria were detached with trypsin, and the samples were washed in dH_2O and in absolute ethanol and soaked in dH_2O to reduce the number of free ions remaining as a result of the buffer. Finally, the liquid on the sample was removed using N_2 gas. To ensure that the surfaces were well cleaned of cells and bacteria, the samples were imaged using a Hitachi SEM FE 4800 field emission SEM.

8.5.1 X-ray photoelectron spectroscopy (XPS) (VI)

The planar DLC and Ti samples subjected to the MSC or *S. aureus* cultures were analysed using a high-resolution X-ray photoelectron spectrometer (PHI 5600). To interpret the XPS data, the linear least-squares fit of Gaussian functions was applied to the O, N and C spectra (Matlab).

8.5.2 Time-of-flight secondary ion mass spectrometry (VI)

Time-of-flight secondary ion mass spectrometry (ToF-SIMS) experiments were performed for the planar DLC and planar and patterned Ti substrates subjected to the MSC and *S. aureus* cultures and both types of co-cultures. Positive and negative static SIMS measurements were performed using a ToF-SIMS spectrometer (ION-TOF, Munster). The samples were irradiated with a pulsed 25 keV Bi^{3+} liquid-metal ion beam.

A limited peak set was constructed using unique amino acid fragmen-

Table 8.4. List of characteristic secondary ion fragments cleaved off from the amino acids.

Mass	Formula	Amino acids	Mass	Formula	Amino acids
45	CHS	Cya	87	$C_3H_7N_2O$	Asn
47	CH_3S	Cys	88	$C_3H_6NO_2$	Asn
54	C_3H_4N	His	91	C_7H_7	Phe, Tyr
55	C_3H_3O	Tyr	95	$C_5H_7N_2$	His
58	C_2H_4NO	Gly	98	$C_4H_4NO_2$	Asn
	C_3H_8N	Glu	100	$C_4H_{10}N_3$	Arg
59	CN_3H_5	Arg	102	$C_4H_8NO_2$	Glu
60	C_2H_6NO	Ser	104	$C_4H_{10}NS$	Met
61	C_2H_5S	Met	107	C_7H_7O	Tyr
68	C_4H_6N	Pro	110	$C_5H_8N_3$	His
69	C_4H_5O	Thr	113	$C_4H_5N_2O_2$	Gly
71	$C_3H_3O_2$	Ser	115	$C_4H_7N_2O_2$	Gly
72	C_3H_6NO	Gly	120	$C_8H_{10}N$	Phe
	$C_4H_{10}N$	Val	121	$C_6H_5N_2O$	His
73	$C_2H_7N_3$	Arg	127	$C_5H_{11}N_4$	Arg
74	C_3H_8NO	Thr	129	$C_5H_{13}N_4$	Gln
81	$C_4H_5N_2$	His	130	$C_9H_8N_6$	Trp
82	$C_4H_6N_2$	His	131	C_9H_7O	Phe
83	C_5H_7O	Val	132	C_9H_8O	Phe
84	C_4H_6NO	Gln, Glu	136	$C_8H_{10}NO$	Tyr
	$C_5H_{10}N$	Lys	159	$C_{10}H_{11}N_2$	Trp
85	$C_3H_5N_2O$	Gly	170	$C_{11}H_8NO$	Trp
86	$C_5H_{12}N$	Ile, Leu			

tation patterns from ToF-SIMS data that had previously been identified as characterising proteins (Table 8.4). The peak areas for each spectrum were then normalised to the intensity of the sum of the selected peaks to account for fluctuations in the secondary ion yield between the various spectra. The data from culture medium was subtracted from the cell data. Principal component analysis (PCA) was applied to analyse the ToF-SIMS spectra (Matlab) of the MSC and bacteria footprints. The coefficients obtained from the PCA were further applied to the co-culture data.

8.6 Statistical analysis (I–VI)

All numerical results are expressed as the mean $\pm$ the standard deviation (of the mean). The statistical significance of the differences observed between groups was evaluated using one-way analysis of variance followed by Tukey HSD Post-Hoc Tests (I-III) or a Mann Whitney test (Matlab; V).

9. Results and Discussion

9.1 Surface characterisation of micro-patterned surfaces (I–III)

The roughness, surface energy and surface charge of the planar and square-patterned DLC, Cr, Ta and Ti surfaces were measured.

9.1.1 Surface roughness

The planar DLC, Cr, Ta and Ti coatings had an average surface roughness (R_a) of less than 2 nm, *i.e.* the surfaces were smooth and they had a mirror finish (Fig. 9.1). The R_a and the peak-to-valley roughness (R_{pv}) values of the DLC coatings were the lowest ($p < 0.001$), and the Cr coatings had lower values than the Ta and Ti coatings ($p < 0.001$). Nevertheless, the differences in the R_a values were minor (< 2 nm). It thus seems that the only relevant topographical cue for the substrates studied here is the step (height difference) between the patterns and the background (200 nm). Therefore, it is unlikely that the clear-cut differences seen in the cellular behaviour cultured on various substrates would have been due to the differences in the surface topography. Instead, the differences observed, which will be discussed later, seemed to be mediated by the different chemical compositions of the studied substrates and the physical patterns on the substrates.

9.1.2 Contact angles

Micro-patterning significantly affected the wettability properties of the substrates, *i.e.* the water contact angles were decreased and the diiodomethane contact angles were increased compared to their planar counterparts (Fig. 9.1). However, the differences in the water contact angles be-

tween the samples were relatively small (statistically significantly lower on patterned DLC compared to planar DLC, $p < 0.05$). All of the materials had water contact angles between 63° and 71° except for the Si substrate, which had a water contact angle of 32°. In contrast, the variation in the diiodomethane contact angles was statistically significant; the diiodomethane contact angles were clearly higher on the patterned surfaces (46°−49°) than on their planar counterparts (33°−38°, $p < 0.05$). Due to these differences, the patterned substrates had a lower dispersive surface energy, γ_S^D, component and higher polar, γ_S^P, and total, γ_S, surface energy components than their planar counterparts ($p < 0.05$ for all of them, except the γ_S of DLC). This variation in the surface energy can explain some of the differences observed in the cellular responses to these substrates, which will be discussed later (Section 9.2.2).

9.1.3 Zeta potential

Further surface analysis was conducted by measuring the streaming currents. The planar DLC substrate had the most negatively charged surface layer ($p < 0.001$, Fig. 9.1), whereas the planar Cr and Ti substrates had the highest ζ-potential values ($p < 0.001$). The ζ-potential values of the patterned substrates were approximately between the values of their planar counterparts and those of the Si substrate. It was also found that the coating method affected the surface charge of the material significantly. The ζ-potential for the laser-ablated DLC was higher (-54.5±0.6 mV, VI) than for the FPAD-DLC (-70.2±1.1 mV, I–III).

The surface charge affects protein adsorption, and a link between the ζ-potential value and amino acid adsorption was also observed in this study, as discussed in Section 9.5.2.

9.2 SaOS-2 cells and MSCs on micro-patterned surfaces (I–III)

The adhesion and spreading of osteoblastic SaOS-2 cells and MSCs on micro-patterned substrates were studied and it was found that micropatterning can be used for controlling cells. The results suggest that the osseointegration of implants could be modulated by changing the monotonous implant-host interface into a micro-patterned interface to provide physical cues for cells.

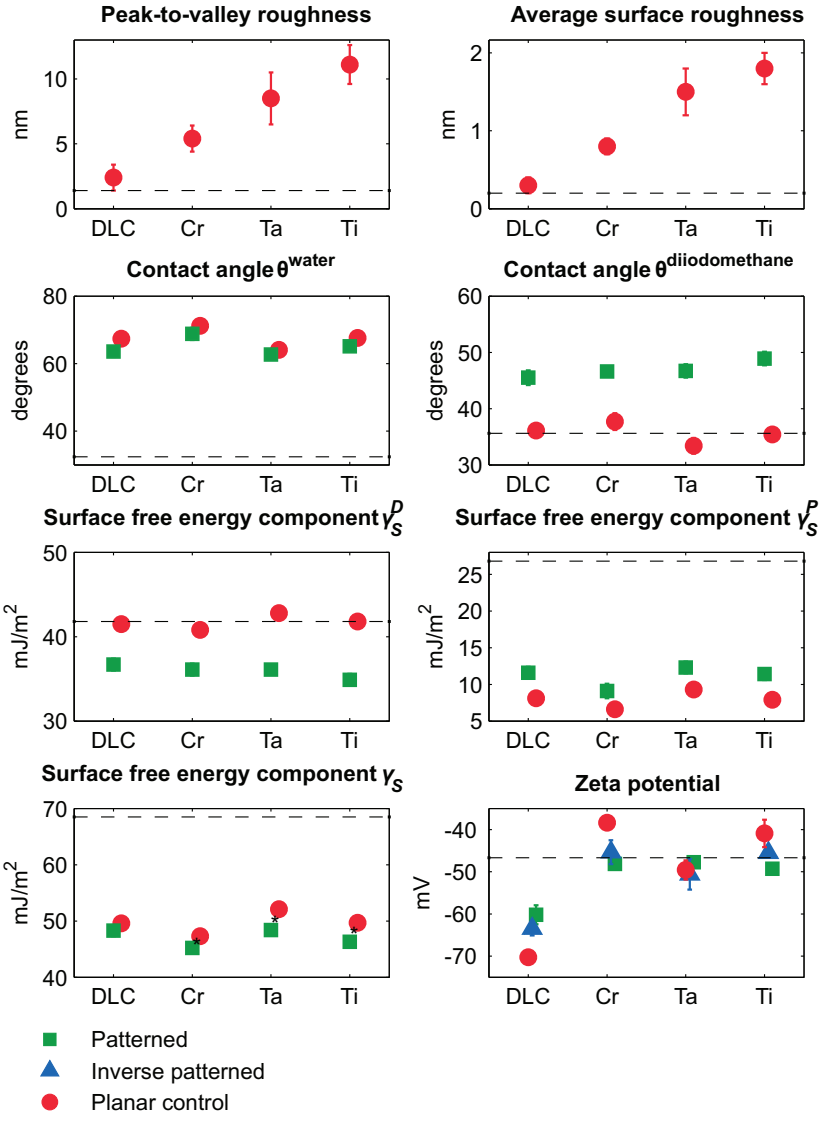

Figure 9.1. Surface properties of the micro-patterned substrates. First row: peak-to-valley roughness (R_{pv}) and average surface roughness (R_a) of the materials. Second row: contact angles of water and diiodomethane. Third row: the surface energy components γ_S^D and γ_S^P. Fourth row: the surface energy component γ_S and the ζ-potential values. The dotted line in the graphs marks the value for the Si substrate.

9.2.1 Adhesion and spreading on micro-patterned surfaces (I, II)

SaOS-2 cells were cultured on patterned substrates containing three different sizes of patterns composed of DLC, Cr, Ta or Ti on a Si background or *vice versa* (8.1 A and B). The cells clearly preferred the coating material

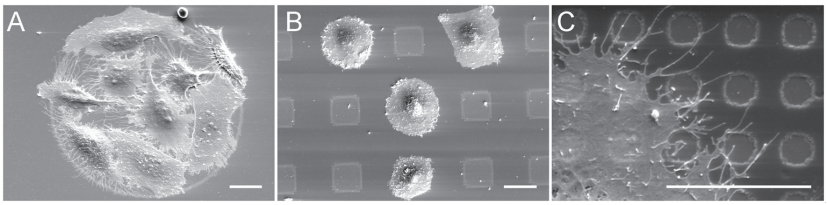

Figure 9.2. Alignment of the SaOS-2 cells on the (A) large and (B) medium biomaterial patterns; (C) the small Si patterns demonstrate a cellular preference for the biomaterial coating over the Si surfaces at 48 h.

over Si, which was demonstrated in three different ways (Fig. 9.2). First, SaOS-2 cells adhered to and spread quite well on the large rectangular (sides 125 µm) or circular (diameter 125 µm) patterns, the size of which made it possible for several cells to adhere to one pattern. The shape of the pattern controlled the adherence and spreading of the cells and the boundaries of the outermost cells followed the edge of the coating, aligning themselves along the edges.

Second, on medium-sized patterns (25 µm sides or diameter) that were smaller than the area of an individual cell, the shape of the adhered cells no longer conformed strictly to the shape of the pattern. Each cell usually covered only one pattern, although the cells on adjacent biomaterial islands now tended to be in partial contact with each other. A few cells stretched from one pattern to another over an inter-island distance of 15 µm, giving these cells elongated, branched or star-like shapes. On the inverse samples, the cells attached themselves to the coated background and had an elongated appearance when they passed through the narrow passages between the patterns, *e.g.* the narrowest passages were only 15 µm between the circular patterns.

Third, on substrate areas containing small square (5 µm) or circular (5 µm) patterns, the individual patterns were too small to accommodate a single cell, and so the cells seemingly non-selectively stretched over larger areas covering several islands. However, at their outer edges, the cells sent out thin and slender filopodia (or microspikes), which seemed to prefer the coating material while trying to circumvent and avoid the bare Si substrate.

The cellular preference for the biomaterial coating over the Si substrate was quantified on the patterned substrates with large squares (sides 75 µm or 100 µm, Fig. 9.3, Fig. 9.4). On average, the density of the SaOS-2 cells on the coating was 330% higher than on the Si background (900±80 *vs.* 210±20 cells/mm^2, $p < 0.001$) and the coverage was 80% higher (72±4%

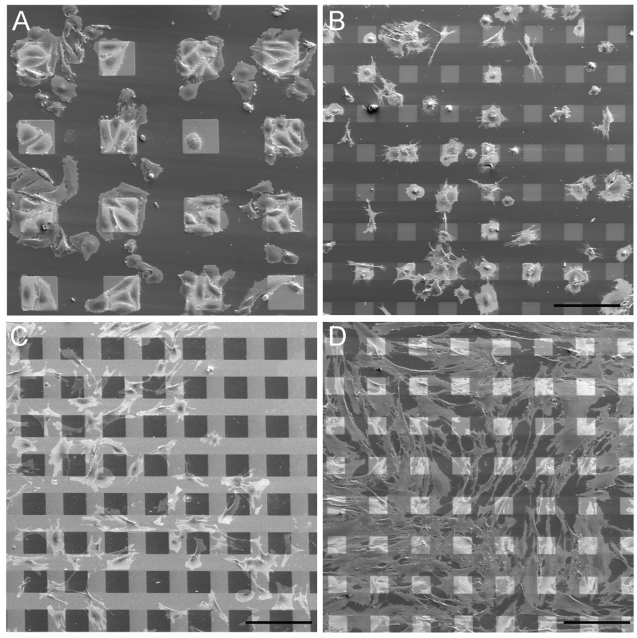

Figure 9.3. SEM images of cells on micro-patterned surfaces: (A) SaOS-2 cells at 48 h on a patterned substrate, (B) MSCs at 7.5 h on a patterned substrate, (C) MSCs at 7.5 h on an inverse-patterned substrate and (D) MSCs at 5 d on a patterned substrate. The scale bar is 200 µm.

vs. 40±2%, $p < 0.001$). Likewise, the density of MSCs on the coatings was 150% higher than on the Si background (108±16 *vs.* 43±6 cells/mm^2, $p < 0.001$) and the coverage on the coatings was 23% higher than on the Si background (32±5% *vs.* 26±2%, $p < 0.001$) at 7.5 h. Naturally, this preference was lost when the cells had grown and were nearly confluent. At 5 d, the coverage of the MSCs was only marginally higher on the coatings than on the Si background (76±5% *vs.* 71±3%, p=0.06).

On the inverted surfaces, the density and coverage of the MSCs were approximately 200% higher on the coating than on the Si patterns at 7.5 h (83±5 cells/mm^2 *vs.* 26±2 cells/mm^2 and 59±2% *vs.* 20±3%; $p < 0.001$). Again, the difference was lost at 5 d (67±4% *vs.* 65±2%; p=0.123).

The preference of SaOS-2 cells for the coatings over the Si background was confirmed by immunofluorescence staining of the actin cytoskeleton, which was well organised in cells on the coated islands but poorly organised in cells adhering to the Si background (Fig. 9.5). This organisation of the actin cytoskeleton in cells lying on the coating was probably the result of the formation of vinculin-containing adhesion plaques (focal adhesions), which were predominantly seen in the cells on the coated patterns, but which were only present in low numbers in cells lying on the Si

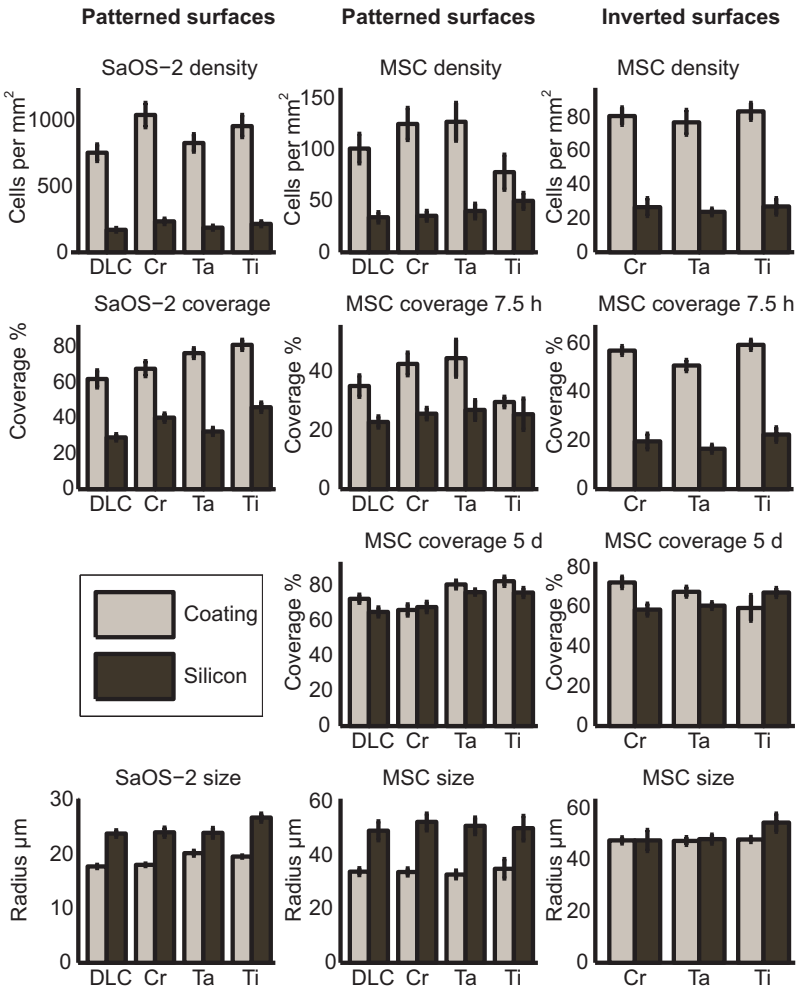

Figure 9.4. The density, coverage and size of the cells on micro-patterned surfaces. First column, SaOS-2 cells on patterned surfaces; second column, MSCs on patterned surfaces; and third column, MSCs on inverse-patterned surfaces. First row, the density of the cells; second and third rows, the coverage of the cells at various time points; fourth row, the size of the cells.

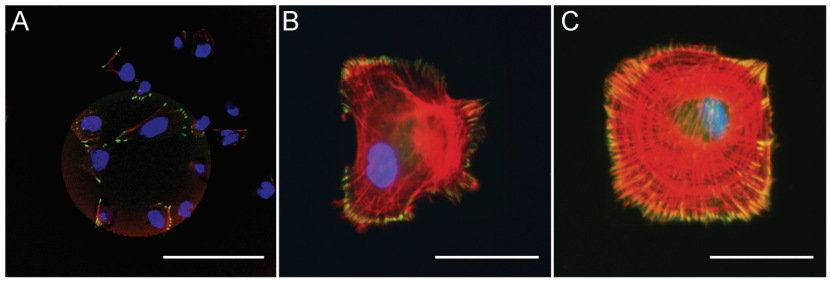

Figure 9.5. Actin-vinculin staining of cells on micro-patterned surfaces: (A) SaOS-2 cells, (B,C) MSC. The scale bar is 50 µm.

background.

The MSCs did not show a similar preference for cytoskeletal organisation. Interestingly, the MSCs had already started to spread out, attaching themselves mostly to the corners of the square patterns at 7.5 h. A previous study demonstrated that the cells preferentially extended lamellipodia, filopodia and microspikes from the corners of the stamped ECM islands (Parker *et al.*, 2002). Here, a similar effect of different surface chemistries without any adhesion-promoting coating was demonstrated. This phenomenon could be exploited to guide the migration of the cells.

The patterns had a strong effect on the size of the cells. The radius of SaOS-2 cells was 15% smaller on the coated islands than on the Si background (19.9±0.4 µm *vs.* 23.5±0.8 µm $p < 0.001$). Likewise, The radius of the MSCs on the coated islands was 33% smaller than on the Si background (34±2 µm *vs.* and 51±4 µm $p < 0.001$). No such differences in size were observed on the inverse-patterned surfaces (radius 48±1 µm on the coated background and 50±3 µm on the Si patterns, $p=0.24$).

The effect on the cell size is a critical factor in, for example, stem cell differentiation. Previous research has demonstrated that adhesive patterns on an anti-adhesive background regulate the size of the cells (McBeath *et al.*, 2004). Here, the same effect was demonstrated primarily due to different surface chemistries; while both enable cell adhesion, one of them is more cytocompatible than the other.

9.2.2 Osteogenesis on micro-patterned surfaces (II, III)

The osteogenic differentiation of MSCs on the square-patterned substrates (Fig. 8.1 C, D) was compared to the differentiation on the planar substrates. The differentiation was evaluated using colorimetric measurements, stainings and the RNA expression measurements of osteogenic markers.

The early osteogenic marker ALP was highly expressed at both the enzyme activity level and the mRNA on the square-patterned and inverse square-patterned Ti surfaces of the osteogenically induced MSC cultures at 14 d (Fig. 9.6, $p < 0.03$ against the uninduced cellular controls). This could indicate that, in particular, the combination of Ti as the cellular substrate and the patterning favours a rapid onset of bone formation. This supports the general idea that Ti is a biocompatible implant material, which is easily osseointegrated and therefore commonly used in bone-integrating implants (Boyan *et al.*, 2001).

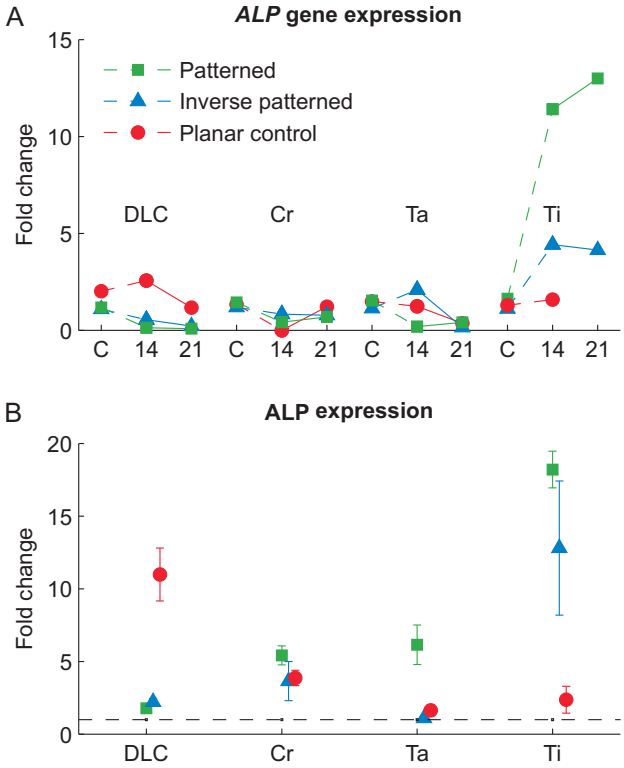

Figure 9.6. ALP activity on micro-patterned surface: (A) colorimetric measurement at 14 d (mean + SEM) and (B) gene expression of ALP; undifferentiated MSCs (C) and osteogenically induced MSCs at 14 d (14) and osteogenically induced MSCs at 21 d (21).

All three mid-term markers, RUNX2, SMAD1 and OP, showed parallel profiles, which clearly contradict the initial interpretation mentioned above. Even though, the gene expression levels on Ti were higher compared to the expression levels on DLC and Cr, the inverse square-patterned and/or the planar Ta-samples clearly had the highest expression for these mid-term markers ($p < 0.02$ compared to all the other materials; Fig. 9.7).

At first, it seems somewhat paradoxical that ALP was so much higher on the square-patterned and the inverse square-patterned Ti samples than on the corresponding Ta samples, but this can be explained by the transient expression of ALP over the early phase of bone formation and its subsequent down-regulation during the intermediate phase of bone formation (Jaiswal *et al.*, 1997). This is compatible with the concept that Ta is also a bone-friendly biomaterial (Bobyn *et al.*, 1999).

Finally, the late-phase osteogenesis marker, bone mineral formation, clearly showed that MSCs were successfully induced for osteoblasts capa-

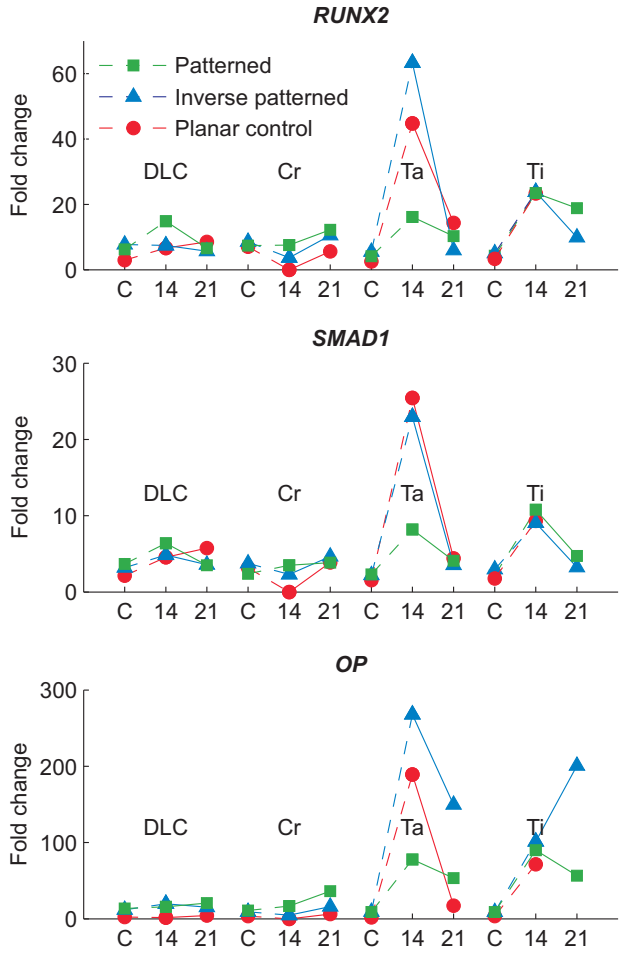

Figure 9.7. The gene expression of the mid-term osteogenic markers, RUNX2, SMAD1 and OP, on the micro-patterned surfaces: undifferentiated MSCs (C) and osteogenically induced MSCs at 14 d (14) and osteogenically induced MSCs at 21 d (21).

ble of producing a mineralised bone matrix. All of the samples except for planar Cr ($p = 0.27$) had statistically significantly higher values than the uninduced control cells ($p < 0.01$). This is important because, in contrast to the early and mid-term labile or transient markers, this late-phase osteogenesis marker is not transient in this cellular differentiation assay; rather, it is permanent, which makes it possible to draw two firm conclusions.

First, the formation of a mineralised bone matrix confirms that the induced cells passed all the early and mid-term differentiation stages and reached a late differentiation state characterised by bone mineral deposition. The poor performance of the planar Cr samples was not unex-

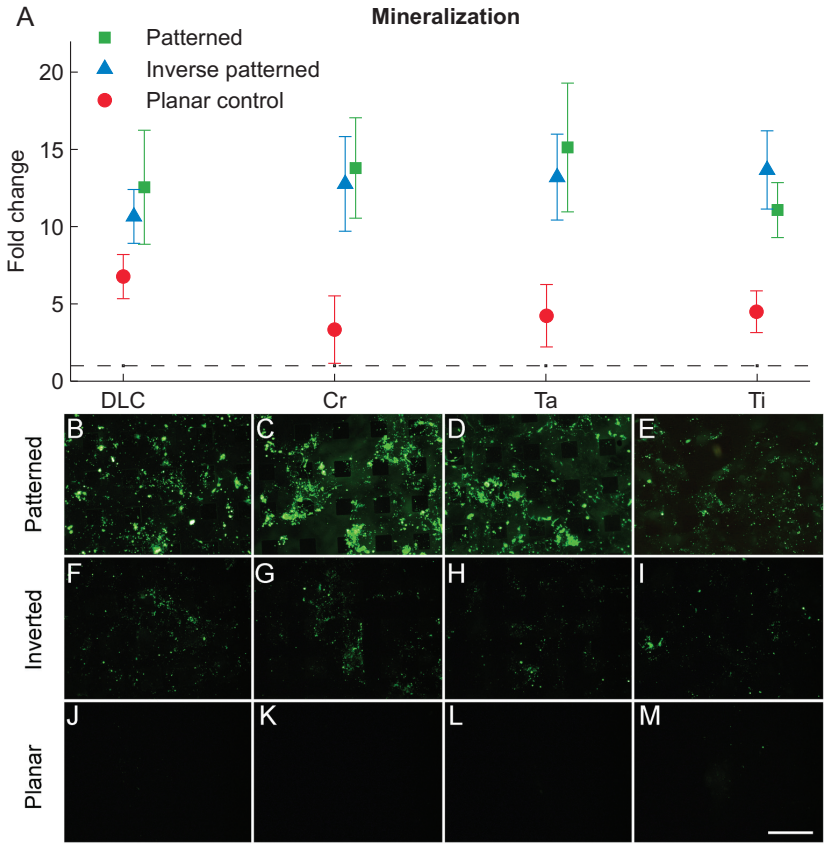

Figure 9.8. Hydroxyapatite on micro-patterned surfaces at 28 d: (A) colorimetric measurement (dotted line marks the negative control) and (B–M) staining of hydroxyapatite. The scale bar is 200 µm.

pected: pure Cr, in contrast to Cr alloys such as CoCrMo, is not a biomaterial. Intriguingly, the patterning enabled bone mineral formation even on the Cr-containing cell-unfriendly samples. Second, the mineralisation studies confirm the most significant conclusion of this study: the square-patterned and inverse square-patterned samples performed better than any of the planar samples (Fig. 9.8 A; $p < 0.001$). Moreover, the density of the cells was lower on both types of patterned substrates than on the planar substrates (2900 *vs.* 4800 cells/cm^2; $p < 0.04$), which resulted in an even larger difference in the amount of minerals formed per cell than was demonstrated in Fig. 9.8.

It could be speculated that the pattern edge phenomenon caused the differences. Pattern edges influence cell division, the cell cytoskeleton and migration (Théry *et al.*, 2006; Jiang *et al.*, 2005; Hoover *et al.*, 2008; Chan and Yousaf, 2008; Brock *et al.*, 2003) and may play a role in MSC differentiation, with the geometry of the patterns influencing the adipogenesis of

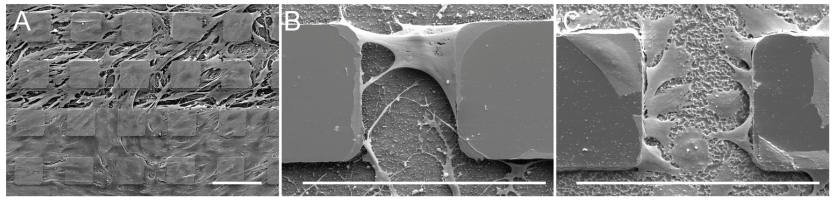

Figure 9.9. SEM on 3D surfaces: (A) MSCs on 20 µm pillars (upper-half) and 5 µm pillars (bottom half) at 5 d; (B) fibroblast extending from one 20 µm high pillar to another at 5 d; (C) SaOS-2 cells reaching from the interspace of the 20 µm pillars to the top of the pillars at 48 h. The scale bar is 200 µm

the MSCs (Luo *et al.*, 2008) and the timing of the differentiation (Chaubey *et al.*, 2008). However, as shown later 200 nm high patterns on the homogeneous surface chemistry had no significant effect on cell adhesion or osteogenesis (Section 9.3.1).

Another significant feature of the patterned samples was that they had a lower dispersive surface energy component, but a higher polar surface energy component, than their planar counterparts ($p < 0.05$). Surface heterogeneities facilitate multiple protein adsorption mechanisms and enable the heterogeneous and versatile distribution and orientation of proteins (Edmiston and Saavedra, 1998). Consequently, it can be concluded that the osteogenesis that was promoted on the patterned surfaces was not regulated by the pattern edges, but that the variation in the surface chemistry and energy might, at least in part, explain why patterning the surfaces improved the mineralisation process.

9.3 Effect of 3D pillar surfaces on cells (IV)

The hypothesis was that, compared to conventional 2D cultures, substrates containing 3D nano- and micron-sized pillars would also allow cells to grow at the third dimension and help them attach to and extend from top-to-top or top-to-bottom, thereby activating their cytoskeleton to promote osteogenesis. The adhesion of MSCs, fibroblasts and SaOS-2 cells, as well as the osteogenic differentiation of MSCs, was evaluated. The planar Si, TiO_2 and DLC substrates were compared to 200 nm, 5 µm and 20 µm high pillars. MSCs were additionally cultured on Ormocomp®, and the results indicate that Ormocomp® can potentially be used in cellular applications.

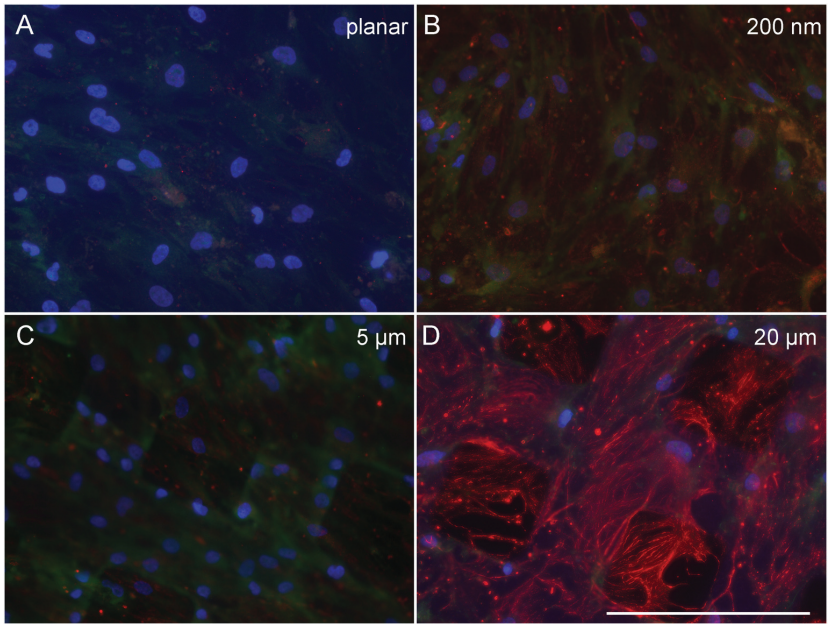

Figure 9.10. Staining of ERK (red), ROCK (green) and nuclei (blue) on a 3D DLC substrate at 21 d. The scale bar is 200 µm.

9.3.1 Adhesion of MSCs, fibroblasts and SaOS-2 cells onto 3D pillars

MSCs and fibroblasts growing in 3D networks demonstrated the ability to adhere to pillar edges and stretched between the adhesion contacts over 100 µm distances (Fig. 9.9 A, B). SaOS-2 cells, which are only about half the size of the MSCs or fibroblasts, adhered to 3D pillars by assuming a flat shape and growing as individual cells on horizontal or vertical substrate surfaces (Fig. 9.9 C).

As expected, the stretching of the cells between the pillars resulted in activation of the cytoskeleton. As the result, the staining of ERK was strongest on 20 µm pillars (Fig. 9.10). Both the non-induced and induced cells behaved similarly (on DLC and Si at 14 and 21 d). The ROCK expression was not significantly affected by the pillars, but an enhancement was seen in induced cells compared to non-induced cells (not shown).

The results for TiO_2 were different from those obtained using DLC and Si. Bone nodule formation was observed already at 14 d. These nodules were easily washed away. However, the remaining cell-clusters expressed both ERK and ROCK quite strongly, with there being no significant differences between the substrate areas. Nonetheless, the 20 µm high pillars seemed to inhibit the cell-cell interactions and the formation of cell clus-

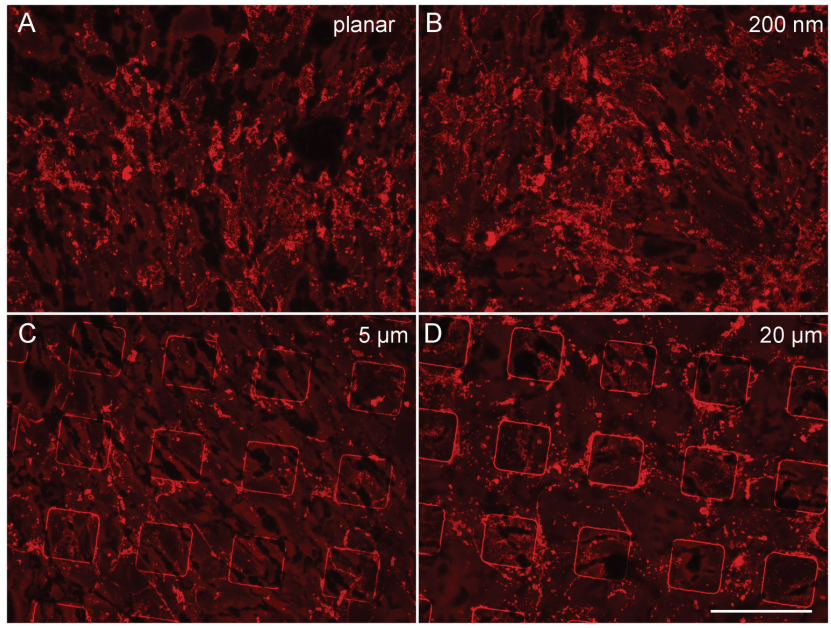

Figure 9.11. Alizarin Red staining on 3D Si substrate at 28 d. The mineralisation is equal in all areas. The scale bar is 200 µm

ters was delayed.

9.3.2 Osteogenic differentiation on 3D pillars

Unexpectedly, the success of osteogenesis was dominated by the cytocompatibility of the substrate across the 3D structure. This was shown with the successive development of the early ALP, intermediate OP and late mineralization markers, together with bone nodule formation, which were seen in planar and low profile (200 nm and 5 µm) TiO_2 pillars but which were rare in the 20 µm landscape.

All of the osteogenic markers (ALP, OP and mineralization) showed parallel results. For the Si and DLC substrates, the staining was random on the planar substrate and 200 nm pillars (Fig. 9.11). For the 5 µm pillars, the staining was slightly promoted and some organisation of the cells was apparent, with the cells preferring the interspaces of the pillars instead of the tops of the pillars. This difference was even more evident on the 20 µm pillars.

The results were different for the TiO_2 substrate than for the DLC and Si substrates (Fig. 9.12). Significant cluster formation with strong staining was observed on the planar TiO_2 surface and low-profile pillar surfaces (200 nm and 5 µm). The OP stain appeared as a ring around these

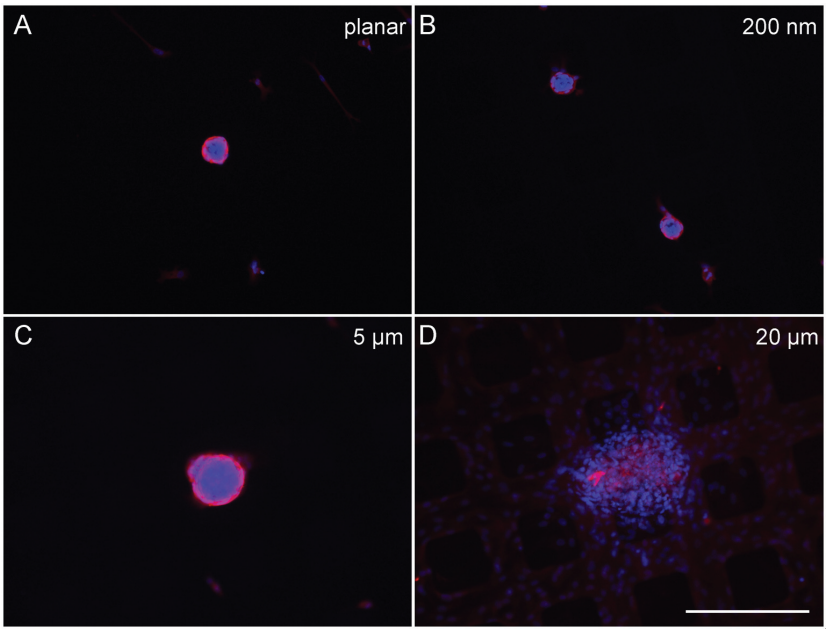

Figure 9.12. Osteopontin (red) and nuclear (blue) staining on a 3D Ti substrate at 21 d. The cluster formation is strong on the planar and low-profile pillar surfaces and clearly delayed in the high 20 µm pillar area. The scale bar is 200 µm.

clusters, whereas both ALP and mineralization stained the whole cluster matrix. No cluster formation was found in the 20 µm pillar substrates at 14 d and only a relatively few formations were found at the later time points. Instead, staining for the 20 µm pillars appeared similar on all the substrate materials (Si, TiO_2 and DLC): there was clear but not overly strong staining of the osteogenic markers in the interspaces of the pillars and hardly any staining on the tops of the pillars. In places where the cluster formation was evident, there was stronger staining.

The MSCs grew to confluence in 2D cultures, with extensive cell-cell contacts at their periphery, which allowed for intercellular communication; in contrast, the 3D pillars cells were stretched between two or more of their substrate contact points, with most of their cellular surface bathing in cell culture fluid and being devoid of direct cell–cell contacts. Cytoskeletal tension has been described to enhance osteogenesis (McBeath *et al.*, 2004) but also cell-cell communication through gap junctions is required for the full maturation of osteoblasts (Ferrari *et al.*, 2000; Schiller *et al.*, 2001; Li *et al.*, 1999). Here, the lack of intercellular contacts seems to halt the osteogenesis promoting effects of the cytoskeletal tension.

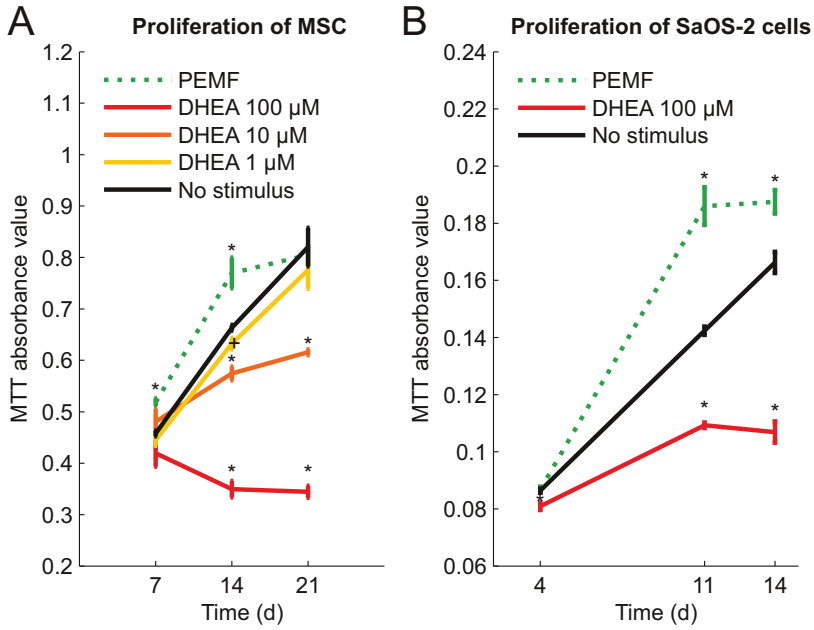

Figure 9.13. Proliferation rate of (A) MSCs and (B) SaOS-2 cells stimulated with PEMF or DHEA. Statistically significant differences compared to the control cells are marked with a star (*, $p < 0.001$), or with a plus-sign (+, $p < 0.05$). The data are represented as a mean ± standard error of the mean.

9.4 The effect of PEMF and DHEA on MSCs and SaOS-2 cells (V)

The effects of PEMF and DHEA stimuli on the proliferation of SaOS-2 cells and MSCs and on the osteogenic differentiation of MSCs were evaluated. The PEMF stimulus promoted the proliferation rate of both cell types, whereas the DHEA stimulus promoted the induced osteogenesis of MSCs.

9.4.1 The effect of PEMF on cells

The PEMF stimulus increased the proliferation rate of SaOS-2 cells compared to the non-stimulated cells by 30% at 11 d ($p < 0.001$), but the difference narrowed to 13% at 14 d ($p < 0.01$), at the time when the cells reached confluence (Fig. 9.13). Similarly, the PEMF stimulus increased the proliferation rate of MSCs compared to the non-stimulated cells by 13% at 7 d and by 16% at 14 d ($p < 0.001$), but the difference dissipated when the cells reached confluence at 21 d. The PEMF stimulus had no major effects on osteogenesis at a seeding density of 3000 cells/cm^2 (Fig. 9.14), which is a relatively low seeding density.

The findings related to the increased proliferation rate of MSCs under

PEMF stimulus are supported by Sun *et al.* (2009). The contradictory results, *e.g.* delayed proliferation (Tsai *et al.*, 2009), can be explained by the different PEMF stimulation used in their experiments (see Table 4.1, the stimulus used here is the same as was used by Jansen *et al.* 2010). Osteogenesis seems to be dependent on the intensity and pulse duration of the PEMF stimulation (Matsunaga *et al.*, 1996) and, hence, it is logical to find various proliferation rates in response to different stimulation protocols.

Nevertheless, Jansen *et al.* (2010) used a similar PEMF stimulus to the one used here, but found inhibited proliferation and induced differentiation of bone marrow-derived MSCs. A reasonable explanation for this apparent contradictory result pertains to the initial seeding density that was used. Jansen *et al.* (2010) used a high seeding density for the MSCs, *i.e.* 10 000 cells/cm^2, which impairs the spreading of MSCs so that they cannot develop tension in their cytoskeleton between the local adhesions; this results in a condition that is favourable for adipogenesis (Spiegelman and Ginty, 1983; McBeath *et al.*, 2004). In contrast, a lower seeding density, *e.g.* 3000 cells/cm^2, which was the density used here, makes it possible for the cells to spread so that they can exert tension in their cytoskeleton; this then promotes osteogenesis (Carvalho *et al.*, 1998; Thomas *et al.*, 2002; McBeath *et al.*, 2004). Hence, it seems that the seeding density is important for the outcome of the PEMF stimulation. Concurrently, Schwartz *et al.* (2008, 2009) suggest that PEMF increases the post-confluence osteogenesis of MSCs. It seems that PEMF can support the pre-confluence proliferation and post-confluence osteogenic differentiation of MSCs. This conclusion is further supported by the ALP peak of PEMF-stimulated MSCs at 21 d, which indicates a delayed promoting effect on osteogenesis (Fig. 9.14).

9.4.2 The effect of DHEA on cells

The osteoblast responses of MSCs to sex hormones vary widely depending on the donor of the stem cells (Leskelä *et al.*, 2006). Two individuals, a female and a male, were studied and both showed similar responses to the DHEA stimulus. In contrast to the PEMF stimulus, the DHEA stimulus suppressed the proliferation rate of SaOS-2 cells and MSCs and promoted the osteogenic differentiation of MSCs. 100 µM DHEA treatment decreased the proliferation rate of SaOS-2 cells by 5% compared to non-stimulated cells at 4 d ($p < 0.01$) and by 36% at 14 d ($p < 0.001$). For MSCs, the suppressing effect was not significant at 7 d, but very clear and

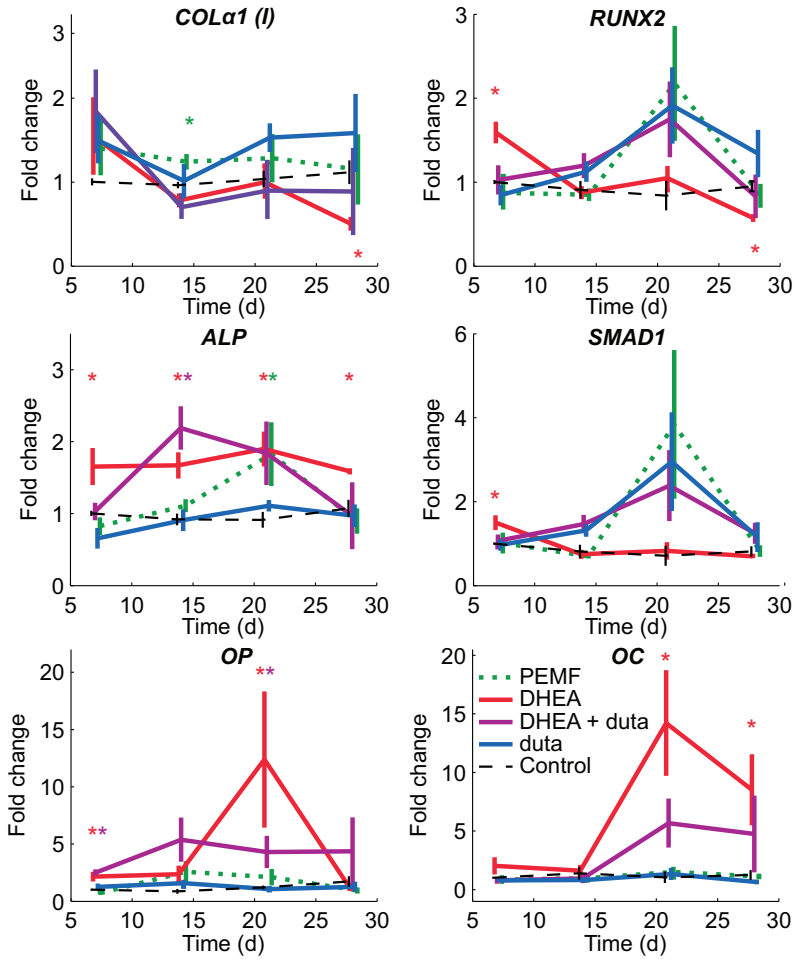

Figure 9.14. Expression of the osteogenic markers of MSCs induced to osteogenesis. PEMF had no significant effect on osteogenesis. DHEA increased all other markers except COLα1. Dutasteride inhibited the effect of DHEA (DHEA + duta), but dutasteride treatment alone (duta) had no significant effect on osteogenesis. Statistically significant differences ($p < 0.05$) are denoted with a star sign (*).

dose-dependent at 14 d (47%, $p < 0.001$ for 100 µM DHEA; 13%, $p < 0.001$ for 10 µM DHEA; and 6% $p < 0.05$ for 1 µM DHEA; Fig. 9.13). For higher concentrations of DHEA, the difference was clear at 21 d (58% for 100 µM and 25% for 10 µM; $p < 0.001$), but no longer significant for a concentration as low as 1 µM DHEA because the cells had reached confluence.

The DHEA stimulus clearly promoted the osteogenesis of osteogenically induced MSCs (Fig. 9.14). A minor enhancement was observed in the staining of early and mid-term markers (ALP, OP and OC) and mineralization was significantly increased (Fig. 9.15). The ALP gene expression of DHEA-stimulated cells increased throughout the experiment compared

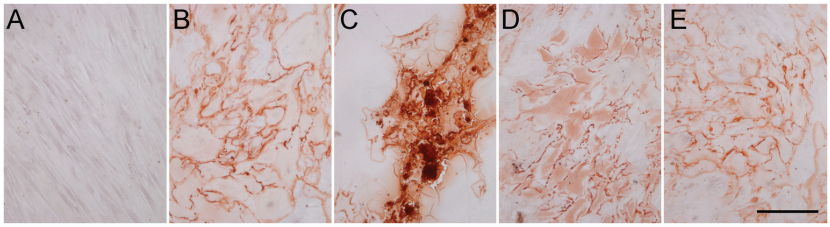

Figure 9.15. Alizarin Red S staining of DHEA-treated MSCs at 28 d. Panel (A) shows the non-induced control cells, panel (B) the osteogenically induced control cells, panel (C) the DHEA-treated cells, panel (D) the DHEA- and dutasteride-treated cells and panel (E) dutasteride-treated cells. The scale bar is 200 µm.

to non-stimulated cells (fold chance 1.7; $p < 0.04$). RUNX2 and SMAD1 peaked higher than the control at 7 d (fold change 1.6 and 1.5; $p < 0.008$), whereas the OP and OC expression peaked at 21 d (fold change 12.4; $p < 0.008$ and 14.2; $p < 0.02$). Dutasteride inhibited the effect of DHEA. The ALP expression of the DHEA-stimulated cells in the presence of dutasteride was statistically significantly increased compared to the control only at 14 d ($p < 0.02$). Furthermore, the RUNX2, SMAD1 and OC expression of DHEA and dutasteride-treated cells was not significantly different from the control cells and, although the OP expression at 21 d was significantly higher compared to the control ($p < 0.008$), it was lower than the expression of OP in DHEA-treated cells (fold change 4.3 *vs.* 12.4 compared to control). In addition, mineralisation staining confirmed that dutasteride blocked the osteogenesis-promoting effect of DHEA. The dutasteride treatment alone caused no statistically significant cellular changes compared to the control. This indicates that the DHEA-to-DHT pathway had been completed and that the DHEA had been conversed into DHT in MSCs by a 5α-reductase-dependent pathway.

In addition, the DHEA stimulus increased the OP and OC mRNA levels of non-induced MSCs in a conversion independent way, since the effect was not suppressed by dutasteride. However, no corresponding osteogenesis-promoting effect was seen in any staining.

The osteogenesis-promoting effect of the DHEA stimulus could be expected because functionally active sex steroids play a key role in bone metabolism and androstenetriol, an active metabolite of DHEA, has been shown to promote the osteogenic differentiation of MSCs (Malik *et al.*, 2010).

These results suggest that a sequential use of mitogenic PEMF early in the fracture healing or implant integration process, followed by a later

administration of a DHEA stimulus with an osteogenic differentiating effect, might be worthwhile in a randomised clinical trial.

9.5 Footprint analysis (VI)

It was hypothesised that the molecular composition of the mammalian ECM and bacterial extracellular polymeric substance (EPS) differ to such an extent that modern and sensitive spectroscopic methods would enable their specific identification based on the cell-free footprints left on the implant surface subsequent to an effective removal of whole live and dead eukaryotic and bacterial cells.

The MSCs, *S. aureus* and co-cultures of the two were cultured on the biomaterial substrates. The viability of *S. aureus* in MSCGM was confirmed by live-dead staining, and crystal violet staining verified that the amount of EPS produced by *S. aureus* was not affected by the media. Furthermore, the live-dead staining showed that some MSCs had survived in co-culture type 2, where the MSCs had been let to adhere for 48 h prior to the addition of *S. aureus*. In co-culture type 1, where the MSCs and *S. aureus* were added simultaneously, all of the MSCs had detached subsequent to a 96 h incubation period. Although most of the MSCs had detached from the surface, they had left their 'permanent' footprint on the surface.

Prior to the spectroscopy measurements, the surfaces were verified so that they were cleaned of cells and bacteria by imaging the surfaces with SEM.

9.5.1 XPS analysis of the footprint of MSC and *S. aureus*

In general, the XPS spectra exhibited peaks resulting from oxygen, carbon and nitrogen, and naturally, the spectra of Ti2p on the Ti samples. A few differences were observed between the samples, but they were not large enough to discriminate of the *S. aureus* samples from the MSC samples. This was not unexpected due to the relatively non-descript nature of XPS compared to SIMS analysis of protein-adhered surfaces (Wagner and Castner, 2001; Canavan *et al.*, 2005).

9.5.2 ToF-SIMS analysis of the footprint of MSC and *S. aureus*

Previous experiments have applied ToF-SIMS to cellular material and have successfully discriminated various yeast strains (Jungnickel *et al.*,

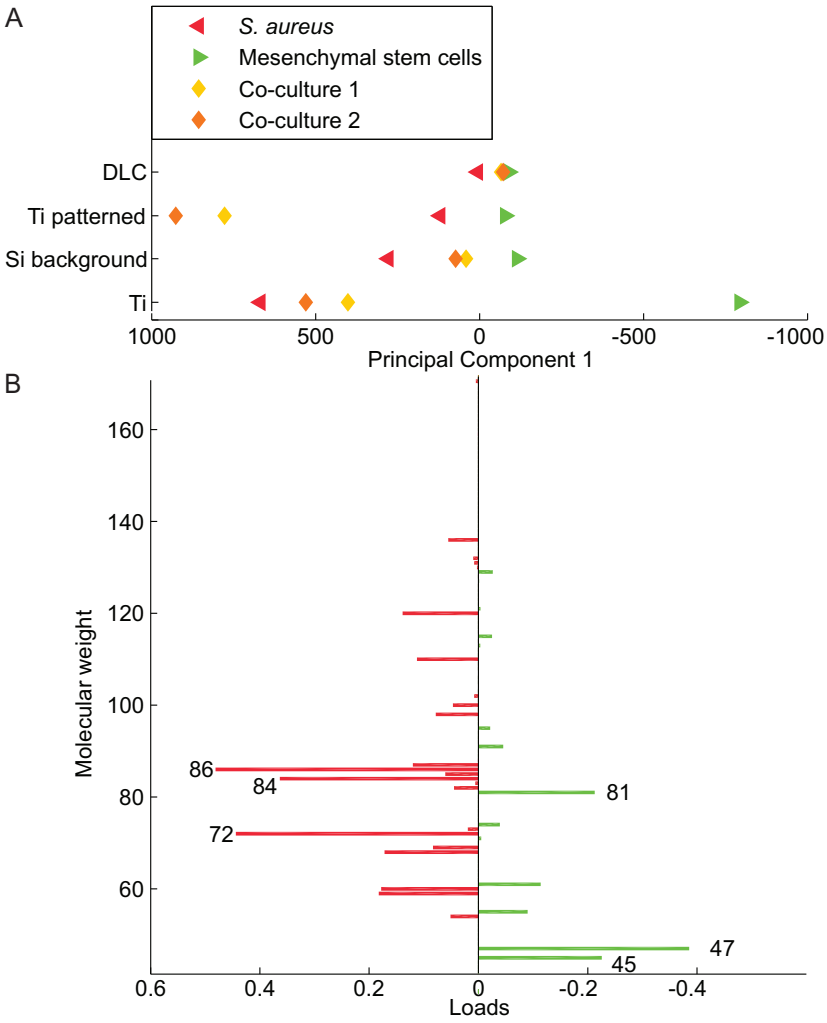

Figure 9.16. (A) The PCA of the ToF-SIMS data made it possible to clearly separate the MSC samples from the *S. aureus* samples and the co-culture samples; (B) the loadings define the size of the contribution of each original variable to the PCs.

2005) and a variety of breast cancer cell types (Kulp *et al.*, 2006). These studies, however, only examined the actual cellular material, whereas the aim here was to discriminate the infected surfaces from the non-infected surfaces subsequent to carefully detaching all of the cellular material.

The PCA of the ToF-SIMS data allowed for clear overall separation ($p < 0.03$) of the *S. aureus* and co-culture samples from the MSC samples (Fig. 9.16 A, representative samples). The differences were predominantly observed in principal component (PC) 1, which accounted for 66% of the statistical separation of the total variance between all of the samples.

It was observed that the peaks at m/z 72 (C_3H_6NO, glycine, $C_4H_{10}N$

valine), 84 ($C_5H_{10}N$ lysine, C_4H_6NO glutamine / glutamic acid) and 86 ($C_5H_{12}N$, leucine / isoleucine) accounted for the majority of the loading on the *S. aureus* side of the PC 1 axis, while the peaks at m/z 45, 47 (CHS, CH_3S cysteine) and 81 ($C_4H_5N_2$, histidine) accounted for the majority of the loading on the side of the PC 1 axis attributed to the MSC samples (Fig. 9.16 B). In addition, a clear structure of the main histidine component (m/z 110 $C_5H_8N_3$) was observed on the MSC samples.

Logically, the PCA values of the co-cultures were located between the values of the pure MSC samples and those of the pure *S. aureus* samples. Moreover, co-culture type 1 (started with MSC culture) was further away from *S. aureus* than co-culture type 2 (to which MSC and staphylococci were added simultaneously), with one exception. The Ti patterns showed a much stronger *S. aureus* footprint in the co-cultures than in the pure *S. aureus* culture.

Previous experiments have shown that MSCs and *S. aureus* spread better on Ti surfaces than on DLC surfaces (II, Myllymaa *et al.* 2013). This better adherence and growth of both types of cells on the cell-friendly and sticky Ti may in part explain why the MSC and *S. aureus* footprints were more easily differentiated on the Ti samples than on the DLC samples.

Another potential explanation for the differences between the TOF-SIMS footprints is that the Ti surface binds more proteins and amino acids than the Si background and that the DLC surface binds less of these components than the Si background. This was demonstrated by the ToF-SIMS images of the patterned DLC and Ti samples, where the total ion count was significantly higher on the Ti patterns than on the Si background, whereas the total ion count was lower on the DLC-patterns than on the Si background. The surface charge may affect the binding of some proteins and amino acid on these surfaces. Indeed, evidence has recently been presented that a parabolic relationship exists between the protein adsorption and zeta potential when a wide zeta potential range is taken into consideration (Kaivosoja *et al.*, 2012).

This research provides a new option for studying how the surfaces of revision-operated (exchanged) clinical implants eventually show the footprints of bacteria and eukaryotic cells, even in bacterial culture negative cases. However, these results are preliminary and further studies of implants removed from patients are required.

10. General Discussion and Conclusions

The main aim of this study was to find methods to potentially improve the osseointegration of implants. The first part of the work focused on material-oriented approaches. It was shown that even partially patterned DLC, Ti, Ta and Cr coatings enhanced the cytocompatibility of silicon surfaces. Osteogenesis was improved on the patterned coatings compared to the planar coatings probably due to pattern-dependent changes in the surface energy. The edge and shape of the pattern may also regulate the spread and differentiation of the cells; however, Publication IV demonstrated that sole patterning with homogeneous surface chemistry had no significant effect on the spread or osteogenic differentiation of MSCs. Although several studies have shown that activation of the cell cytoskeleton promotes osteogenesis, that alone is not enough. In Publication IV, a strong activation of the cell cytoskeleton on 20 µm pillar and suppressed osteogenesis was shown. This was probably due to inhibited cell–cell interaction and an inability to form cell clusters, which are necessary for the initiation of bone formation. Materials that support the formation of adhesion molecules, premature osteoblast clustering and cell–cell communication have been shown to enhance the differentiation and mineralization activity of osteoblasts (Miron *et al.*, 2011). Cell–cell interactions may be responsible for the enhancement of osteogenic differentiation on patterned surfaces, which was observed in Publication III. The density of the cells on the patterns was 150–200% higher compared to the density on the background at an early point in time. The concentration of cells on the patterns might initiate cell clustering, which is necessary for further osteogenic differentiation. Furthermore, this hypothesis is supported by the fact that on patterned titanium, the improvement in hydroxyapatite formation was the smallest (Fig. 9.8) and also the increase in cell density was the smallest (Fig. 9.4). However, the true role of the surfaces on cell–cell interactions still needs to be studied.

Two other potentially important external factors, namely PEMF and DHEA, were investigated. Previous research on the effects of PEMF has

been somewhat inconsistent. This was partly due to the differences in the PEMF signals used in the experiments. The results presented here indicated that the proliferation of MSCs was promoted at a low seeding density level (3000 cells/cm^2), which is commonly recommended for osteogenic studies, but that no significant effect on osteogenesis was observed. This is exactly opposite of the result reported by Jansen *et al.* (2010). It is concluded that the PEMF stimulus in question can stimulate the pre-confluence proliferation of MSCs and their post-confluence osteogenic differentiation.

Publication V concluded that DHEA suppressed the proliferation rate of MSCs and promoted their osteogenic differentiation. This was partly due to the conversion of DHEA to DHT, but some other effects played a role as well; for instance, non-osteogenically induced MSCs showed enhanced expression of OP and OC despite blocking the DHEA to DHT conversion with a 5α-reductase inhibitor. These results suggest that a sequential use of mitogenic PEMF early during the fracture healing or implant integration, followed by a later administration of DHEA with an osteogenic differentiating effect, might be worth studying in a randomised clinical trial. The treatment could be specifically beneficial for osteoporotic patients whose condition may challenge the fixation of a prosthesis. However, to improve the currently used procedures, many patients and a very long follow-up may be required. This treatment could be beneficial also for tissue engineering and regenerative medicine applications, such a bioabsorbable implants in the fixation of fractures (Törmälä and Rokkanen, 2001) or in the reconstruction of bone defects (Mesimäki *et al.*, 2009).

The first part of the thesis focused on improving bone regeneration on an implant surface. In addition to the regeneration of the tissue, the capability to avoid bacterial adhesion, colonisation, biofilm formation and subsequent chronic infection-induced inflammation, which may cause tissue necrosis, is necessary for osseointegration. Last, but not least, it was demonstrated that ToF-SIMS is a potential tool for discriminating between bacterial and eukaryotic acellular footprints (the rests of an extracellular polymeric substance and ECM, respectively) and may have potential in the *post-hoc* diagnosis of colonization, biofilm formation and implant-related infections, even in culture-negative cases. New methods for infection diagnostics are needed because the current methods are not totally reliable and it is crucial to understand the reasons for implant failure in order to develop better implant materials in the future.

Bibliography

Arvidson K, Abdallah BM, Applegate LA *et al.* (2011) *Bone regeneration and stem cells*. J Cell Mol Med 15:718–746.

Barradas AMC, Yuan H, van Blitterswijk CA *et al.* (2011) *Osteoinductive biomaterials: current knowledge of properties, experimental models and biological mechanisms.* Eur Cell Mater 21:407–429.

Bassett CAL, Pawluk RJ and Pilla AA (1974) *Acceleration of fracture repair by electromagnetic fields. A surgically noninvasive method.* Ann N Y Acad Sci 238:242–262.

Benedetto AD, Watkins M, Grimston S *et al.* (2010) *N-cadherin and cadherin 11 modulate postnatal bone growth and osteoblast differentiation by distinct mechanisms.* J Cell Sci 123:2640–2648.

Benoit DSW, Schwartz MP, Durney AR *et al.* (2008) *Small functional groups for controlled differentiation of hydrogel-encapsulated human mesenchymal stem cells.* Nat Mater 7:816–823.

Biggs MJP, Richards RG, Gadegaard N *et al.* (2009) *The use of nanoscale topography to modulate the dynamics of adhesion formation in primary osteoblasts and ERK/MAPK signalling in STRO-1+ enriched skeletal stem cells.* Biomaterials 30:5094–5103.

Bobyn JD, Stackpool GJ, Hacking SA *et al.* (1999) *Characteristics of bone ingrowth and interface mechanics of a new porous tantalum biomaterial.* J Bone Joint Surg Br 81:907–914.

Boix T, Gómez-Morales J, Torrent-Burgués J *et al.* (2005) *Adsorption of recombinant human bone morphogenetic protein rhBMP-2m onto hydroxyapatite.* J Inorg Biochem 99:1043–1050.

Bovenberg SA, van Uum SHM and Hermus ARMM (2005) *Dehydroepiandrosterone administration in humans: evidence based?* Neth J Med 63:300–304.

Boyan BD, Dean DD, Lohmann CH *et al.* (2001) Titanium in medicine, chap. The titanium-bone cell interface in vitro: The role of the surface in promoting osteointegration, 561–586. Springer.

Brammer KS, Oh S, Cobb CJ *et al.* (2009) *Improved bone-forming functionality on diameter-controlled TiO(2) nanotube surface.* Acta Biomater 5:3215–3223.

Brock A, Chang E, Ho CC *et al.* (2003) *Geometric determinants of directional cell motility revealed using microcontact printing.* Langmuir 19:1611–1617.

Canalis E (2008) *Notch signaling in osteoblasts*. Sci Signal 1:pe17.

Canavan HE, Cheng X, Graham DJ *et al.* (2005) *Cell sheet detachment affects the extracellular matrix: a surface science study comparing thermal liftoff, enzymatic, and mechanical methods.* J Biomed Mater Res A 75:1–13.

Canning MO, Grotenhuis K, de Wit HJ *et al.* (2000) *Opposing effects of dehydroepiandrosterone and dexamethasone on the generation of monocyte-derived*

dendritic cells. Eur J Endocrinol 143:687–695.
Carré A and Lacarriére V (2008) Contact angle, wettability and adhesion, vol. 5, chap. Cell adhesion to polystyrene substrates: Relevance of interfacial free energy, 253–267. VSP, Leiden, the Netherlands.
Carré A and Lacarriére V (2010) *How substrate properties control cell adhesion. A physical–chemical approach*. J Adh Sci Tech 24:815–830.
Carvalho RS, Schaffer JL and Gerstenfeld LC (1998) *Osteoblasts induce osteopontin expression in response to attachment on fibronectin: demonstration of a common role for integrin receptors in the signal transduction processes of cell attachment and mechanical stimulation.* J Cell Biochem 70:376–390.
Cavalcanti-Adam EA, Volberg T, Micoulet A *et al.* (2007) *Cell spreading and focal adhesion dynamics are regulated by spacing of integrin ligands.* Biophys J 92:2964–2974.
Chan EWL and Yousaf MN (2008) *A photo-electroactive surface strategy for immobilizing ligands in patterns and gradients for studies of cell polarization.* Mol Biosyst 4:746–753.
Chang WHS, Chen LT, Sun JS *et al.* (2004) *Effect of pulse-burst electromagnetic field stimulation on osteoblast cell activities.* Bioelectromagnetics 25:457–465.
Chaubey A, Ross KJ, Leadbetter RM *et al.* (2008) *Surface patterning: tool to modulate stem cell differentiation in an adipose system.* J Biomed Mater Res B 84:70–78.
Chung DJ, Castro CHM, Watkins M *et al.* (2006) *Low peak bone mass and attenuated anabolic response to parathyroid hormone in mice with an osteoblast-specific deletion of connexin43.* J Cell Sci 119:4187–4198.
Clerici M, Trabattoni D, Piconi S *et al.* (1997) *A possible role for the cortisol/anticortisols imbalance in the progression of human immunodeficiency virus.* Psychoneuroendocrinology 22:S27–S31.
Costerton J, Geesey G and Cheng K (1978) *How bacteria stick.* Sci Am 238:86–95.
Costerton J, Stewart P and Greenberg E (1999) *Bacterial biofilms: a common cause of persistent infections.* Science 284:1318–1322.
Curtis A and Wilkinson C (2001) *Nantotechniques and approaches in biotechnology.* Trends Biotechnol 19:97–101.
Curtis AS and Varde M (1964) *Control of cell behavior: Topological factors*. J Natl Cancer Inst 33:15–26.
Dalby MJ, Gadegaard N, Tare R *et al.* (2007) *The control of human mesenchymal cell differentiation using nanoscale symmetry and disorder.* Nat Mater 6:997–1003.
Dalby MJ, McCloy D, Robertson M *et al.* (2006) *Osteoprogenitor response to defined topographies with nanoscale depths.* Biomaterials 27:1306–1315.
Darouiche RO (2001) *Device-associated infections: a macroproblem that starts with microadherence.* Clin Infect Dis 33:1567–1572.
Darouiche RO (2004) *Treatment of infections associated with surgical implants.* N Engl J Med 350:1422–1429.
Davies JE, Causton B, Bovell Y *et al.* (1986) *The migration of osteoblasts over substrata of discrete surface charge.* Biomaterials 7:231–233.
Dimitriou R and Babis GC (2007) *Biomaterial osseointegration enhancement with biophysical stimulation.* J Musculoskelet Neuronal Interact 7:253–265.
Diniz P, Shomura K, Soejima K *et al.* (2002a) *Effects of pulsed electromagnetic field (PEMF) stimulation on bone tissue like formation are dependent on the maturation stages of the osteoblasts.* Bioelectromagnetics 23:398–405.
Diniz P, Soejima K and Ito G (2002b) *Nitric oxide mediates the effects of pulsed electromagnetic field stimulation on the osteoblast proliferation and differenti-*

ation. Nitric Oxide 7:18–23.

Edmiston PL and Saavedra SS (1998) *Molecular orientation distributions in protein films: III. Yeast cytochrome c immobilized on pyridyl disulfide-capped phospholipid bilayers.* Biophys J 74:999–1006.

Fan SK, Huang PW, Wang TT *et al.* (2008) *Cross-scale electric manipulations of cells and droplets by frequency-modulated dielectrophoresis and electrowetting.* Lab Chip 8:1325–1331.

Feng B, Weng J, Yang BC *et al.* (2003) *Characterization of surface oxide films on titanium and adhesion of osteoblast.* Biomaterials 24:4663–4670.

Ferrari SL, Traianedes K, Thorne M *et al.* (2000) *A role for N-cadherin in the development of the differentiated osteoblastic phenotype.* J Bone Miner Res 15:198–208.

Fujibayashi S, Neo M, Kim HM *et al.* (2004) *Osteoinduction of porous bioactive titanium metal.* Biomaterials 25:443–450.

Fujita K and Janz S (2007) *Attenuation of WNT signaling by DKK-1 and -2 regulates BMP2-induced osteoblast differentiation and expression of OPG, RANKL and M-CSF.* Mol Cancer 6:71.

Fukumoto S, Hsieh CM, Maemura K *et al.* (2001) *Akt participation in the Wnt signaling pathway through Dishevelled.* J Biol Chem 276:17479–17483.

Gingell D and Todd I (1980) *Red blood cell adhesion. II. Interferometric examination of the interaction with hydrocarbon oil and glass.* J Cell Sci 41:135–149.

Griffin XL, Warner F and Costa M (2008) *The role of electromagnetic stimulation in the management of established non-union of long bone fractures: what is the evidence?* Injury 39:419–429.

Grinnell F and Feld MK (1982) *Fibronectin adsorption on hydrophilic and hydrophobic surfaces detected by antibody binding and analyzed during cell adhesion in serum-containing medium.* J Biol Chem 257:4888–4893.

Guntur AR, Rosen CJ and Naski MC (2012) *N-cadherin adherens junctions mediate osteogenesis through PI3K signaling.* Bone 50:54–62.

Gómez-Barrena E, Esteban J, Medel F *et al.* (2012) *Bacterial adherence to separated modular components in joint prosthesis: A clinical study.* J Orthop Res 30:1634–1639.

Hall BK and Miyake T (2000) *All for one and one for all: condensations and the initiation of skeletal development*. BioEssays 22:138–147.

Harding G, Mak YT, Evans B *et al.* (2006) *The effects of dexamethasone and dehydroepiandrosterone (DHEA) on cytokines and receptor expression in a human osteoblastic cell line: potential steroid-sparing role for DHEA.* Cytokine 36:57–68.

Hartig M, Joos U and Wiesmann HP (2000) *Capacitively coupled electric fields accelerate proliferation of osteoblast-like primary cells and increase bone extracellular matrix formation in vitro.* Eur Biophys J 29:499–506.

Hartkamp A, Geenen R, Godaert GLR *et al.* (2004) *The effect of dehydroepiandrosterone on lumbar spine bone mineral density in patients with quiescent systemic lupus erythematosus.* Arthritis Rheum 50:3591–3595.

Hoover DK, Chan EWL and Yousaf MN (2008) *Asymmetric peptide nanoarray surfaces for studies of single cell polarization.* J Am Chem Soc 130:3280–3281.

Ilvesaro J and Tuukkanen J (2003) *Gap-junctional regulation of osteoclast function.* Crit Rev Eukaryot Gene Expr 13:133–146.

Jaiswal N, Haynesworth SE, Caplan AI *et al.* (1997) *Osteogenic differentiation of purified, culture-expanded human mesenchymal stem cells in vitro.* J Cell Biochem 64:295–312.

Jansen JHW, van der Jagt OP, Punt BJ *et al.* (2010) *Stimulation of osteogenic*

differentiation in human osteoprogenitor cells by pulsed electromagnetic fields: an in vitro study. BMC Musculoskelet Disord 11:188.

Jedlicka S, Leavesley S, Little K *et al.* (2007) *Interactions between chemical functionality and nanoscale surface topography impact fi bronectin conformation and neuronal differentiation on model sol-gel silica substrates.* Mater Res Soc Symp Proc 950:D04–13.

Jiang X, Bruzewicz DA, Wong AP *et al.* (2005) *Directing cell migration with asymmetric micropatterns.* Proc Natl Acad Sci U S A 102:975–978.

Jiang Y, Henderson D, Blackstad M *et al.* (2003) *Neuroectodermal differentiation from mouse multipotent adult progenitor cells.* Proc Natl Acad Sci U S A 100:11854–11860.

Jiang Y, Jahagirdar BN, Reinhardt RL *et al.* (2002a) *Pluripotency of mesenchymal stem cells derived from adult marrow.* Nature 418:41–49.

Jiang Y, Vaessen B, Lenvik T *et al.* (2002b) *Multipotent progenitor cells can be isolated from postnatal murine bone marrow, muscle, and brain.* Exp Hematol 30:896–904.

Jungnickel H, Jones EA, Lockyer NP *et al.* (2005) *Application of TOF-SIMS with chemometrics to discriminate between four different yeast strains from the species Candida glabrata and Saccharomyces cerevisiae.* Anal Chem 77:1740–1745.

Kaivosoja E, Barreto G, Levón K *et al.* (2012) *Chemical and physical properties of regenerative medicine materials controlling stem cell fate.* Ann Med 44:635–650.

Kandori K, Horigami N, Kobayashi H *et al.* (1997) *Adsorption of lysozyme onto various synthetic hydroxyapatites*. J Coll Int Sci 191:498–502.

Karp JM, Yeh J, Eng G *et al.* (2007) *Controlling size, shape and homogeneity of embryoid bodies using poly(ethylene glycol) microwells.* Lab Chip 7:786–794.

Keselowsky BG, Collard DM and García AJ (2003) *Surface chemistry modulates fibronectin conformation and directs integrin binding and specificity to control cell adhesion.* J Biomed Mater Res A 66:247–259.

Khang D, Lu J, Yao C *et al.* (2008) *The role of nanometer and sub-micron surface features on vascular and bone cell adhesion on titanium.* Biomaterials 29:970–983.

Khatiwala CB, Kim PD, Peyton SR *et al.* (2009) *ECM compliance regulates osteogenesis by influencing MAPK signaling downstream of RhoA and ROCK.* J Bone Miner Res 24:886–898.

Khosla S, Amin S and Orwoll E (2008) *Osteoporosis in men.* Endocr Rev 29:441–464.

Kilian KA, Bugarija B, Lahn BT *et al.* (2010) *Geometric cues for directing the differentiation of mesenchymal stem cells.* Proc Natl Acad Sci U S A 107:4872–4877.

Komatsu M, Carraway CA, Fregien NL *et al.* (1997) *Reversible disruption of cell-matrix and cell-cell interactions by overexpression of sialomucin complex.* J Biol Chem 272:33245–33254.

Kulp KS, Berman ESF, Knize MG *et al.* (2006) *Chemical and biological differentiation of three human breast cancer cell types using time-of-flight secondary ion mass spectrometry.* Anal Chem 78:3651–3658.

Lai HC, Zhuang LF, Liu X *et al.* (2010) *The influence of surface energy on early adherent events of osteoblast on titanium substrates.* J Biomed Mater Res A 93:289–296.

Lecanda F, Warlow PM, Sheikh S *et al.* (2000) *Connexin43 deficiency causes delayed ossification, craniofacial abnormalities, and osteoblast dysfunction.* J

Cell Biol 151:931–944.

Lehto VP and Virtanen I (1985) *Vinculin in cultured bovine lens-forming cells.* Cell Differ 16:153–160.

Leskelä HV, Risteli J, Niskanen S *et al.* (2003) *Osteoblast recruitment from stem cells does not decrease by age at late adulthood*. Biochem Biophys Res Commun 311:1008–1013.

Leskelä HV, Olkku A, Lehtonen S *et al.* (2006) *Estrogen receptor alpha genotype confers interindividual variability of response to estrogen and testosterone in mesenchymal-stem-cell-derived osteoblasts.* Bone 39:1026–1034.

Li Z, Zhou Z, Yellowley CE *et al.* (1999) *Inhibiting gap junctional intercellular communication alters expression of differentiation markers in osteoblastic cells.* Bone 25:661–666.

Liu XH, Kirschenbaum A, Yao S *et al.* (2007) *Androgens promote preosteoblast differentiation via activation of the canonical Wnt signaling pathway.* Ann N Y Acad Sci 1116:423–431.

Lohmann CH, Schwartz Z, Liu Y *et al.* (2000) *Pulsed electromagnetic field stimulation of MG63 osteoblast-like cells affects differentiation and local factor production.* J Orthop Res 18:637–646.

Long F (2012) *Building strong bones: molecular regulation of the osteoblast lineage.* Nat Rev Mol Cell Biol 13:27–38.

Luo W, Jones SR and Yousaf MN (2008) *Geometric control of stem cell differentiation rate on surfaces.* Langmuir 24:12129–12133.

Lyklema J (1995) Fundamentals of interface and colloid science, vol. II. Solid-liquid interface. Academic Press, London, United Kingdom.

Lönnroos E, Kautiainen H, Karppi P *et al.* (2006) *Increased incidence of hip fractures. A population based-study in Finland.* Bone 39:623–627.

Malik AK, Khaldoyanidi S, Auci DL *et al.* (2010) *5-Androstene-3β, 7β,17β-triol (β-AET) slows thermal injury induced osteopenia in mice: relation to aging and osteoporosis.* PLoS One 5:e13566.

Marculescu CE, Berbari EF, Hanssen AD *et al.* (2005) *Prosthetic joint infection diagnosed postoperatively by intraoperative culture.* Clin Orthop Relat Res 439:38–42.

Marwah A, Marwah P and Lardy H (2002) *Ergosteroids. VI. Metabolism of dehydroepiandrosterone by rat liver in vitro: a liquid chromatographic-mass spectrometric study.* J Chromatogr B Analyt Technol Biomed Life Sci 767:285–299.

Matsunaga S, Sakou T and Ijiri K (1996) *Osteogenesis by pulsing electromagnetic fields (PEMFs): optimum stimulation setting.* In Vivo 10:351–356.

McBeath R, Pirone DM, Nelson CM *et al.* (2004) *Cell shape, cytoskeletal tension, and RhoA regulate stem cell lineage commitment.* Dev Cell 6:483–495.

McBride SH and Tate MLK (2008) *Modulation of stem cell shape and fate A: the role of density and seeding protocol on nucleus shape and gene expression.* Tissue Eng Part A 14:1561–1572.

Mesimäki K, Lindroos B, Törnwall J *et al.* (2009) *Novel maxillary reconstruction with ectopic bone formation by GMP adipose stem cells.* Int J Oral Maxillofac Surg 38:201–209.

Miron RJ, Hedbom E, Ruggiero S *et al.* (2011) *Premature osteoblast clustering by enamel matrix proteins induces osteoblast differentiation through up-regulation of connexin 43 and N-cadherin.* PLoS One 6:e23375.

Myllymaa K, Levon J, Tiainen VM *et al.* (2013) *Formation and retention of staphylococcal biofilms on DLC and its hybrids compared to metals used as biomaterials*. Coll Surf B Biointerf 101:290–297.

Nakamura M, Nagai A, Hentunen T *et al.* (2009) *Surface electric fields increase*

osteoblast adhesion through improved wettability on hydroxyapatite electret. ACS Appl Mater Interfaces 1:2181–2189.

Nakamura S, Kobayashi T and Yamashita K (2004) *Numerical osteobonding evaluation of electrically polarized hydroxyapatite ceramics.* J Biomed Mater Res A 68:90–94.

Nakashima A, Katagiri T and Tamura M (2005) *Cross-talk between Wnt and bone morphogenetic protein 2 (BMP-2) signaling in differentiation pathway of C2C12 myoblasts.* J Biol Chem 280:37660–37668.

Nelson CL, McLaren AC, McLaren SG *et al.* (2005) *Is aseptic loosening truly aseptic?* Clin Orthop Relat Res 437:25–30.

Neut D, van Horn JR, van Kooten TG *et al.* (2003) *Detection of biomaterial-associated infections in orthopaedic joint implants.* Clin Orthop Relat Res 413:261–268.

Oh S, Brammer KS, Li YSJ *et al.* (2009) *Stem cell fate dictated solely by altered nanotube dimension.* Proc Natl Acad Sci U S A 106:2130–2135.

Olivares-Navarrete R, Hyzy S, Wieland M *et al.* (2010) *The roles of Wnt signaling modulators Dickkopf-1 (Dkk1) and Dickkopf-2 (Dkk2) and cell maturation state in osteogenesis on microstructured titanium surfaces*. Biomaterials 31:2015–2024.

Olkku A, Leskinen JJ, Lammi MJ *et al.* (2010) *Ultrasound-induced activation of Wnt signaling in human MG-63 osteoblastic cells.* Bone 47:320–330.

Owens DK and Wendt RC (1969) *Estimation of the surface free energy of polymers*. J Appl Polym Sci 13:1741–1747.

Panousis K, Grigoris P, Butcher I *et al.* (2005) *Poor predictive value of broad-range PCR for the detection of arthroplasty infection in 92 cases.* Acta Orthop 76:341–346.

Parker KK, Brock AL, Brangwynne C *et al.* (2002) *Directional control of lamellipodia extension by constraining cell shape and orienting cell tractional forces.* FASEB J 16:1195–1204.

Pautke C, Schieker M, Tischer T *et al.* (2004) *Characterization of osteosarcoma cell lines MG-63, Saos-2 and U-2 OS in comparison to human osteoblasts.* Anticancer Res 24:3743–3748.

Perälä A (2011) *Lonkka- ja polviproteesit Suomessa 2010*. Tech. rep., National Institute for Health and Welfare.

Pilla A, Fitzsimmons R, Muehsam D *et al.* (2011) *Electromagnetic fields as first messenger in biological signaling: Application to calmodulin-dependent signaling in tissue repair.* Biochim Biophys Acta 1810:1236–1245.

Pittenger MF, Mackay AM, Beck SC *et al.* (1999) *Multilineage potential of adult human mesenchymal stem cells.* Science 284:143–147.

Reyes M and Verfaillie CM (2001) *Characterization of multipotent adult progenitor cells, a subpopulation of mesenchymal stem cells.* Ann N Y Acad Sci 938:231–233.

Rubin CT, McLeod KJ and Lanyon LE (1989) *Prevention of osteoporosis by pulsed electromagnetic fields.* J Bone Joint Surg Am 71:411–417.

Ruiz SA and Chen CS (2008) *Emergence of patterned stem cell differentiation within multicellular structures.* Stem Cells 26:2921–2927.

Ryoo H, Hoffmann H, Beumer T *et al.* (1997) *Stage-specific expression of Dlx-5 during osteoblast differentiation: involvement in regulation of osteocalcin gene expression.* Mol Endocrinol 11:1681–1694.

Sakai Y, Patterson TE, Ibiwoye MO *et al.* (2006) *Exposure of mouse preosteoblasts to pulsed electromagnetic fields reduces the amount of mature, type I collagen in the extracellular matrix.* J Orthop Res 24:242–253.

Salasznyk RM, Klees RF, Williams WA *et al.* (2007) *Focal adhesion kinase signaling pathways regulate the osteogenic differentiation of human mesenchymal stem cells.* Exp Cell Res 313:22–37.

Sawase T, Jimbo R, Baba K *et al.* (2008) *Photo-induced hydrophilicity enhances initial cell behavior and early bone apposition.* Clin Oral Implants Res 19:491–496.

Schenk RK and Buser D (1998) *Osseointegration: a reality.* Periodontol 2000 17:22–35.

Schiller PC, D'Ippolito G, Balkan W *et al.* (2001) *Gap-junctional communication is required for the maturation process of osteoblastic cells in culture.* Bone 28:362–369.

Schwartz Z, Fisher M, Lohmann CH *et al.* (2009) *Osteoprotegerin (OPG) production by cells in the osteoblast lineage is regulated by pulsed electromagnetic fields in cultures grown on calcium phosphate substrates.* Ann Biomed Eng 37:437–444.

Schwartz Z, Simon BJ, Duran MA *et al.* (2008) *Pulsed electromagnetic fields enhance BMP-2 dependent osteoblastic differentiation of human mesenchymal stem cells.* J Orthop Res 26:1250–1255.

Shiri EH, Mehrjardi NZ, Tavallaei M *et al.* (2009) *Neurogenic and mitotic effects of dehydroepiandrosterone on neuronal-competent marrow mesenchymal stem cells.* Int J Dev Biol 53:579–584.

Sillat T, Pöllänen R, Lopes JRC *et al.* (2009) *Intracrine androgenic apparatus in human bone marrow stromal cells.* J Cell Mol Med 13:3296–3302.

Sjöström T, Dalby MJ, Hart A *et al.* (2009) *Fabrication of pillar-like titania nanostructures on titanium and their interactions with human skeletal stem cells.* Acta Biomater 5:1433–1441.

Slemenda C, Hui S, Longcope C *et al.* (1987) *Sex steroids and bone mass. A study of changes about the time of menopause.* J Clin Invest 80:1261–1269.

Spiegelman BM and Ginty CA (1983) *Fibronectin modulation of cell shape and lipogenic gene expression in 3T3-adipocytes.* Cell 35:657–666.

Stains J and Civitelli R (2005a) *Cell-cell interactions in regulating osteogenesis and osteoblast function.* Birth Defects Res C Embryo Today 75:72–80.

Stains JP and Civitelli R (2005b) *Gap junctions in skeletal development and function.* Biochim Biophys Acta 1719:69–81.

Sun LY, Hsieh DK, Yu TC *et al.* (2009) *Effect of pulsed electromagnetic field on the proliferation and differentiation potential of human bone marrow mesenchymal stem cells.* Bioelectromagnetics 30:251–260.

Tabrah F, Hoffmeier M, Gilbert F Jr *et al.* (1990) *Bone density changes in osteoporosis-prone women exposed to pulsed electromagnetic fields (PEMFs).* J Bone Miner Res 5:437–442.

Takemoto M, Fujibayashi S, Neo M *et al.* (2006) *Osteoinductive porous titanium implants: effect of sodium removal by dilute HCl treatment.* Biomaterials 27:2682–2691.

Tamura Y, Takeuchi Y, Suzawa M *et al.* (2001) *Focal adhesion kinase activity is required for bone morphogenetic protein–Smad1 signaling and osteoblastic differentiation in murine MC3T3-E1 cells.* J Bone Miner Res 16:1772–1779.

Théry M, Racine V, Piel M *et al.* (2006) *Anisotropy of cell adhesive microenvironment governs cell internal organization and orientation of polarity.* Proc Natl Acad Sci U S A 103:19771–19776.

Thomas CH, Collier JH, Sfeir CS *et al.* (2002) *Engineering gene expression and protein synthesis by modulation of nuclear shape.* Proc Natl Acad Sci U S A 99:1972–1977.

Tirkkonen L, Halonen H, Hyttinen J *et al.* (2011) *The effects of vibration loading on adipose stem cell number, viability and differentiation towards bone-forming cells.* J R Soc Interface 8:1736–1747.

Tomlins P, Leach R, Vagdama P *et al.* (2005) Surfaces and interfaces for biomaterials, chap. On the topographical characterization of biomaterial surfaces, 693–718. Woodhead Publishing Limited, Cambridge, UK.

Trampuz A and Widmer AF (2006) *Infections associated with orthopedic implants.* Curr Opin Infect Dis 19:349–356.

Trampuz A and Zimmerli W (2006) *Diagnosis and treatment of infections associated with fracture-fixation devices.* Injury 37:S59–S66.

Tsai MT, Li WJ, Tuan RS *et al.* (2009) *Modulation of osteogenesis in human mesenchymal stem cells by specific pulsed electromagnetic field stimulation.* J Orthop Res 27:1169–1174.

Tu X, Joeng KS, Nakayama KI *et al.* (2007) *Noncanonical Wnt signaling through G protein-linked PKCδ activation promotes bone formation*. Dev Cell 12:113–127.

Törmälä P and Rokkanen P (2001) *Bioabsorbable implants in the fixation of fractures.* Ann Chir Gynaecol 90:81–85.

Uludag H, D'Augusta D, Palmer R *et al.* (1999) *Characterization of rhBMP-2 pharmacokinetics implanted with biomaterial carriers in the rat ectopic model.* J Biomed Mater Res 46:193–202.

Valle J, Toledo-Arana A, Berasain C *et al.* (2003) *SarA and not sigmaB is essential for biofilm development by Staphylococcus aureus*. Molecular Microbiology 48:1075–1087.

Vitte J, Benoliel AM, Pierres A *et al.* (2004) *Is there a predictable relationship between surface physical-chemical properties and cell behaviour at the interface?* Eur Cell Mater 7:52–63.

Vogler EA (1998) *Structure and reactivity of water at biomaterial surfaces*. Adv Colloid Interface Sci 74:69–117.

von Mühlen D, Laughlin GA, Kritz-Silverstein D *et al.* (2008) *Effect of dehydroepiandrosterone supplementation on bone mineral density, bone markers, and body composition in older adults: the DAWN trial.* Osteoporos Int 19:699–707.

Välimäki VV, Yrjans JJ, Vuorio EI *et al.* (2005) *Molecular biological evaluation of bioactive glass microspheres and adjunct bone morphogenetic protein 2 gene transfer in the enhancement of new bone formation.* Tissue Eng 11:387–394.

Wagner MS and Castner DG (2001) *Characterization of adsorbed protein films by time-of-flight secondary ion mass spectrometry with principal component analysis*. Langmuir 17:4649–4660.

Wallwork ML, Kirkham J, Chen H *et al.* (2002) *Binding of dentin noncollagenous matrix proteins to biological mineral crystals: an atomic force microscopy study.* Calcif Tissue Int 71:249–255.

Wang L, Wang YD, Wang WJ *et al.* (2007) *Dehydroepiandrosterone improves murine osteoblast growth and bone tissue morphometry via mitogen-activated protein kinase signaling pathway independent of either androgen receptor or estrogen receptor.* J Mol Endocrinol 38:467–479.

Waris V, Waris E, Sillat T *et al.* (2010) *BMPs in periprosthetic tissues around aseptically loosened total hip implants.* Acta Orthop 81:420–426.

Wolf OT and Kirschbaum C (1999) *Actions of dehydroepiandrosterone and its sulfate in the central nervous system: effects on cognition and emotion in animals and humans*. Brain Res Rev 30:264–288.

Xiao G, Gopalakrishnan R, Jiang D *et al.* (2002) *Bone morphogenetic proteins,*

extracellular matrix, and mitogen-activated protein kinase signaling pathways are required for osteoblast-specific gene expression and differentiation in MC3T3-E1 cells. J Bone Miner Res 17:101–110.

Yang Y, Tao C, Zhao D *et al.* (2010) *EMF acts on rat bone marrow mesenchymal stem cells to promote differentiation to osteoblasts and to inhibit differentiation to adipocytes.* Bioelectromagnetics 31:277–285.

Yim EKF, Darling EM, Kulangara K *et al.* (2010) *Nanotopography-induced changes in focal adhesions, cytoskeletal organization, and mechanical properties of human mesenchymal stem cells.* Biomaterials 31:1299–1306.

Yu ZW, Calvert TL and Leckband D (1998) *Molecular forces between membranes displaying neutral glycosphingolipids: evidence for carbohydrate attraction.* Biochemistry 37:1540–1550.

Yun MS, Kim SE, Jeon SH *et al.* (2005) *Both ERK and Wnt/beta-catenin pathways are involved in Wnt3a-induced proliferation.* J Cell Sci 118:313–322.

Zanetti NC and Solursh M (1984) *Induction of chondrogenesis in limb mesenchymal cultures by disruption of the actin cytoskeleton.* J Cell Biol 99:115–123.

Zhang D, Pan X, Ohno S *et al.* (2011) *No effects of pulsed electromagnetic fields on expression of cell adhesion molecules (integrin, CD44) and matrix metalloproteinase-2/9 in osteosarcoma cell lines.* Bioelectromagnetics 32:463–473.

Zimmerli W (2006) *Infection and musculoskeletal conditions: Prosthetic-joint-associated infections.* Best Pract Res Clin Rheumatol 20:1045–1063.

Zimmermann U, Friedrich U, Mussauer H *et al.* (2000) *Electromanipulation of mammalian cells: fundamentals and application.* IEEE Transactions on Plasma Science 28:72–82.

Errata

Publication II

Figure 2 Panel C: colours of the bars should be the opposite, cell radius is smaller on the patterns than on the background.
The step between the biomaterial island and background is 200 nm, not 20 nm as written in p 336.

Aalto-DD 34/2013

ISBN 978-952-60-5038-6
ISBN 978-952-60-5037-9 (pdf)
ISSN-L 1799-4934
ISSN 1799-4934
ISSN 1799-4942 (pdf)

Aalto University
School of Electrical Engineering
Department of Electronics
www.aalto.fi

BUSINESS + ECONOMY

ART + DESIGN + ARCHITECTURE

SCIENCE + TECHNOLOGY

CROSSOVER

DOCTORAL DISSERTATIONS